



Sequential changes in ocean circulation and biological export productivity during the last glacial cycle: a model-data study

Cameron M. O'Neill¹, Andrew McC. Hogg^{1,2}, Michael J. Ellwood¹, Bradley N. Opdyke¹, and Stephen M. Eggins¹

¹Research School of Earth Sciences, Australian National University, Canberra, Australia

²ARC Centre of Excellence for Climate Extremes, Australian National University, Canberra, Australia

Correspondence to: Cameron O'Neill (cameron.oneill@anu.edu.au)

Abstract.

We conduct a model-data analysis of the ocean, atmosphere and terrestrial carbon system to understand their effects on atmospheric CO₂ during the last glacial cycle. We use a carbon cycle box model "SCP-M", combined with multiple proxy data for the atmosphere and ocean, to test for variations in ocean circulation and biological productivity across marine isotope stages spanning 130 thousand years ago to the present. The model is constrained by proxy data associated with a range of environmental conditions including sea surface temperature, salinity, ocean volume, sea ice cover and shallow water carbonate production. Model parameters for global ocean circulation, Atlantic meridional overturning circulation and Southern Ocean biological export productivity are optimised in each marine isotope stage, against proxy data for atmospheric CO₂, $\delta^{13}\text{C}$ and $\Delta^{14}\text{C}$ and deep ocean $\delta^{13}\text{C}$, $\Delta^{14}\text{C}$ and carbonate ion. Our model-data results suggest that global overturning circulation weakened at marine isotope stage 5d, coincident with a ~ 25 ppm fall in atmospheric CO₂ from the penultimate interglacial level. This change was followed by a further slowdown in Atlantic meridional overturning circulation and enhanced Southern Ocean biological export productivity at marine isotope stage 4 (~ 30 ppm). There was also a transient slowdown in Atlantic meridional overturning circulation at MIS 5b. In this model, the last glacial maximum was characterised by relatively weak global ocean and Atlantic meridional overturning circulation, and increased Southern Ocean biological export productivity (~ 20 ppm during MIS 2-4). Ocean circulation and Southern Ocean biology rebounded to modern values by the Holocene period. The terrestrial biosphere decreased by ~ 500 Pg C in the lead up to the last glacial maximum, followed by a period of intense regrowth during the Holocene (~ 750 Pg C). Slowing ocean circulation, a cooler ocean and, to a lesser extent, shallow carbonate dissolution, contributed ~ 75 ppm to atmospheric CO₂ in the ~ 100 thousand-year lead-up to the last glacial maximum, with a further ~ 10 ppm contributed during the glacial maximum. Our model results also suggest that an increase in Southern Ocean biological productivity was one of the ingredients required to achieve the last glacial maximum atmospheric CO₂ level. The incorporation of longer-timescale data into quantitative ocean transport models, provides useful insights into the timing of changes in ocean processes, enhancing our understanding of the last glacial maximum and Holocene carbon cycle transition.



1 Introduction

Large and regular fluctuations in atmospheric CO₂ and ocean proxy signals for carbon isotopes and carbonate ion concentration, over the last 800 kyr, are preserved in ice and marine core records. The most obvious of these fluctuations is the repeated oscillation of atmospheric CO₂ over the range of ~180-280 ppm every ~100 kyr. The magnitude and regularity of these oscillations in atmospheric CO₂, combined with proxy observations for carbon isotopes, point to the quasi-regular transfer of carbon between the main earth reservoirs: the ocean, atmosphere, terrestrial biosphere and marine sediments (Broecker, 1982; Sigman and Boyle, 2000; Toggweiler, 2008; Hogg, 2008; Kohfeld and Ridgwell, 2009; Kohfeld and Chase, 2017). The ocean, given its large size as a carbon store and ongoing exchange of CO₂ with the atmosphere, likely plays the key role in changing atmospheric CO₂ (Broecker, 1982; Knox and McElroy, 1984; Toggweiler and Sarmiento, 1985; Sigman and Boyle, 2000; Kohfeld and Ridgwell, 2009). Ocean-centric hypotheses for variation in atmospheric CO₂ have been examined in great detail for the last glacial maximum (LGM) and Holocene periods, supported by the abundance of paleo data from marine sediment coring and sampling activity (e.g. Sikes et al., 2000; Curry and Oppo, 2005; Kohfeld and Ridgwell, 2009; Oliver et al., 2010; Peterson et al., 2014; Yu et al., 2014b; Menviel et al., 2016; Skinner et al., 2017; Muglia et al., 2018; Yu et al., 2019). However, the hypotheses for variation in atmospheric CO₂ across the LGM-Holocene remain under debate (e.g. Kohfeld et al., 2005; Martinez-Garcia et al., 2014; Menviel et al., 2016; Skinner et al., 2017; Muglia et al., 2018). Hypotheses include ocean biology (e.g. Martin et al., 1987; Martinez-Garcia et al., 2014), ocean circulation (e.g. Burke and Robinson, 2012; Menviel et al., 2016; Skinner et al., 2017) and composite mechanisms (e.g. Kohfeld and Ridgwell, 2009; Hain et al., 2010; Ferrari et al., 2014; Muglia et al., 2018) to explain the LGM-Holocene carbon cycle transition.

Kohfeld and Chase (2017) extended the LGM-Holocene CO₂ debate by evaluating proxy data over the period 18-115 thousand years before present (ka), a time that encompasses the gradual fall in atmospheric CO₂ of ~85-90 ppm from the penultimate interglacial period until the last glacial termination. Kohfeld and Chase (2017) identified time periods during which CO₂ decreased, and aligned these with concomitant changes in proxies for sea surface temperature (SST), sea ice extent, deep Atlantic Ocean circulation and mixing, and ocean biological productivity. Kohfeld and Chase (2017) observed that the ~100kyr transition to the LGM involved three discrete CO₂ events. Firstly, a drop in atmospheric CO₂ of ~35 ppm at ~115-100 ka (marine isotope stage, or MIS, 5c-5d) was accompanied by lower SST and the expansion of Antarctic sea ice cover. A second phase of CO₂ drawdown took place ~72-65 ka (MIS 4-5a), of ~40ppm, and likely resulted from a slowdown in deep ocean circulation (Kohfeld and Chase, 2017). Finally, during the period 40-18 ka (MIS 2-4), atmospheric CO₂ dropped a further 5-10 ppm, which according to Kohfeld and Chase (2017), was the result of enhanced Southern Ocean biological productivity, and continually intensifying deep ocean stratification, including shoaling of North Atlantic Deep Water (NADW) and northward extension of Antarctic Bottom Water (AABW).

In this paper we quantitatively test the Kohfeld and Chase (2017) hypothesis by undertaking model-data experiments in each MIS across the last glacial cycle, and extend their analysis to include Pacific and Indian Ocean modelling and proxy data. We use the SST reconstructions compiled by Kohfeld and Chase (2017) and other glacial cycle proxies presented in that work. We apply a carbon cycle box model (O'Neill et al., 2019), constrained by available atmospheric and oceanic proxy



data, to solve for optimal model-data parameter solutions for ocean circulation and biological export productivity. We also present a qualitative analysis of the compiled proxy data, to place the model-data experiment results in context. We thereby further constrain the timing and magnitude of posited CO₂ mechanisms operating during each MIS in the last glacial cycle (e.g. Kohfeld and Ridgwell, 2009; Oliver et al., 2010; Yu et al., 2013; Eggleston et al., 2016; Yu et al., 2016; Kohfeld and Chase, 2017). This time series analysis complements recent model-data studies of the LGM and Holocene (e.g. Menviel et al., 2016; Kurahashi-Nakamura et al., 2017; Muglia et al., 2018; O'Neill et al., 2019) by testing for changes in the ocean carbon cycle in the lead-up to the LGM, in addition to the LGM-to-Holocene.

2 Materials and methods

2.1 Model description

We used the SCP-M carbon cycle box model in our model-data experiment (O'Neill et al., 2019). SCP-M incorporates the ocean, atmosphere, terrestrial biosphere and marine/continental sediment carbon reservoirs, weathering and river fluxes, and a number of variables including CO₂, phosphorus, alkalinity, carbon isotopes (¹³C and ¹⁴C) and the carbonate ion. SCP-M's fast run time and flexibility renders it useful for long term paleo-reconstructions involving large numbers of quantitative experiments and data integration (O'Neill et al., 2019). In this paper, we extend SCP-M by incorporating a separate basin for the combined Pacific and Indian Oceans (Fig. 1), following the conceptual model of Talley (2013), to incorporate modelling and proxy data for those regions of the ocean. SCP-M is a simple box model, which incorporates large regions of the ocean as averaged boxes and parameterised fluxes. It is an appropriate tool for this study, in which we evaluate many simulations to explore possible parameter combinations, in conjunction with proxy data.

We have added a simple representation of shallow water carbonate fluxes of carbon and alkalinity in SCP-M's low latitude surface boxes, to cater for this feature in theories for glacial cycle CO₂ (e.g. Opdyke and Walker, 1992; Ridgwell et al., 2003), using:

$$\left[\frac{dC_i}{dt} \right]_{reef} = C_{reef} / V_i \quad (1)$$

Where C_{reef} is the prescribed flux of carbon out of/into the low latitude surface ocean boxes during net reef accumulation/dissolution, in mol C yr⁻¹, and V_i is the volume of the low latitude surface box i . The alkalinity flux associated with reef production/dissolution is simply Eq. 1 multiplied by two (e.g. Sarmiento and Gruber, 2006). The model used for this paper is located at <https://doi.org/10.5281/zenodo.3559339>.

2.2 Model-data experiment design

We undertook a series of model-data experiments to solve for the values of ocean circulation and biology parameters at each MIS stage during the last glacial cycle (130-0 ka). We targeted these parameters due to their central role in many LGM-Holocene CO₂ hypotheses (e.g. Knox and McElroy, 1984; Toggweiler and Sarmiento, 1985; Martin et al., 1987; Kohfeld

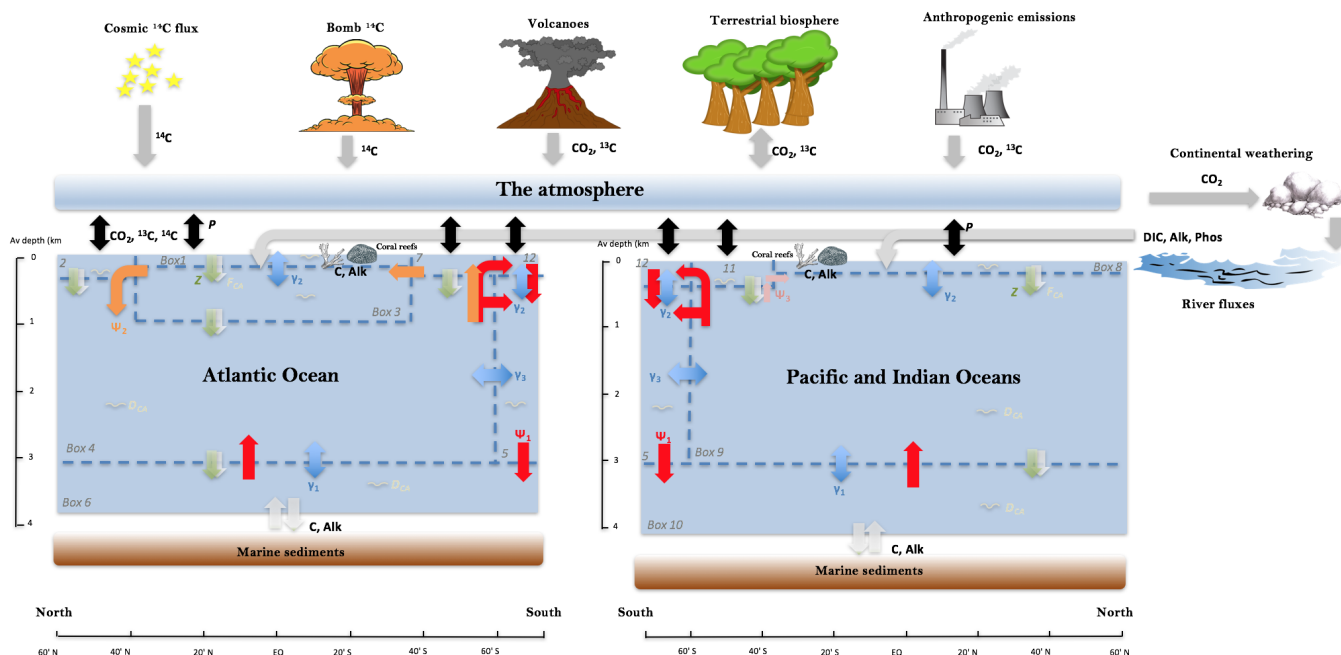


Figure 1. SCP-M configured as a twelve box ocean model-plus atmosphere with marine sediments, continents and the terrestrial biosphere. Exchange of elemental concentrations occur due to fluxes between boxes. Ψ_1 (red arrows) is global overturning circulation (GOC), Ψ_2 (orange arrows) is Atlantic meridional overturning circulation (AMOC). Ψ_3 (pink arrows) is Antarctic intermediate water (AAIW) and Subantarctic mode water (SAMW) formation in the Indian and Pacific Oceans (e.g. Talley, 2013). Blue arrows represent mixing fluxes between boxes. γ_1 and γ_3 parameterise deep-abyssal and Southern Ocean-deep topographically-induced mixing (e.g. De Boer and Hogg, 2014), while γ_2 is low-latitude thermohaline mixing (e.g. Liu et al., 2016). Z (green downward arrows) is the biological pump, F_{CA} (white downward arrows) is the carbonate pump, D_{CA} (white squiggles) is carbonate dissolution and P (black, bidirectional arrows) is the air-sea gas exchange. Key to boxes: Atlantic (box 1: low latitude/tropical surface ocean; box 2: northern surface ocean; box 3: intermediate ocean; box 4: deep ocean; box 6: abyssal ocean; box 7: subpolar southern surface ocean). Pacific-Indian (box 8: low latitude/tropical surface ocean; box 9: deep ocean; box 10: abyssal ocean; box 11: subpolar southern surface ocean). Southern Ocean (box 5: intermediate-deep; box 12: surface ocean). For a more detailed model description see O'Neill et al. (2019) and updated model code and data at <https://doi.org/10.5281/zenodo.3559339>.

and Ridgwell, 2009; Hain et al., 2010; Sigman et al., 2010; Yu et al., 2014a; Menviel et al., 2016; Kohfeld and Chase, 2017; Muglia et al., 2018). We force SST, salinity, sea volume and ice cover, and reef carbonate production, in each MIS, using values sourced from the literature (e.g. Opdyke and Walker, 1992; Key, 2001; Adkins et al., 2002; Ridgwell et al., 2003; Kohfeld and Ridgwell, 2009; Rohling et al., 2009; Wolff et al., 2010; Muscheler et al., 2014; Kohfeld and Chase, 2017). Then, we optimise the model parameters for global overturning circulation (GOC), Atlantic meridional overturning circulation (AMOC) and Southern Ocean biological export productivity in each MIS time slice. We chose GOC and AMOC due to the prevalence of



varying ocean circulation in many theories for glacial cycles of CO₂ (e.g. Sarmiento and Toggweiler, 1984; Toggweiler, 1999; Kohfeld and Ridgwell, 2009; Burke and Robinson, 2012; Freeman et al., 2016; Menviel et al., 2016; Kohfeld and Chase, 2017; Skinner et al., 2017; Muglia et al., 2018), and its key role in distribution of carbon and other elements in the ocean (Talley, 2013). We chose to vary Southern Ocean biological export productivity due to its long-standing place and debate among theories of atmospheric CO₂ during the LGM and Holocene (e.g. Martin et al., 1987; Knox and McElroy, 1984; Sarmiento and Toggweiler, 1984; Sigman and Boyle, 2000; Anderson et al., 2002; Kohfeld and Ridgwell, 2009; Martinez-Garcia et al., 2014; Menviel et al., 2016; Kohfeld and Chase, 2017; Muglia et al., 2018).

The GOC (Ψ_1), AMOC (Ψ_2) and Southern Ocean biology (Z) parameters are varied over ~5,000 possible combinations at each MIS. At the end of each experiment batch, the model results are solved for the best fit to the ocean and atmosphere proxy data using a least-squares optimisation, and the parameter values for Ψ_1 , Ψ_2 and Z are returned. Our experiment time slices are the MIS of Lisiecki and Raymo (2005), with two minor modifications (see Fig. 2). MIS 2 (14-29 ka) as per Lisiecki and Raymo (2005) straddles the LGM (18-24 ka) and the last glacial termination (15-18 ka), while MIS 1 (0-14 ka) incorporates the Holocene period (0-11.7 ka) and the end of the termination. We are interested in the LGM and Holocene as discrete periods, so our experiment time slice for MIS 2 is truncated at 18 ka, and our MIS 1 simply covers the Holocene, removing overlaps with the glacial termination. For MIS 5, we take the timing for peak glacial and interglacial substages of Lisiecki and Raymo (2005), ± 5 kyr for MIS 5c-5e, and ± 2.5 kyr for MIS 5a-5b. Therefore, our modelling excludes the last glacial termination (~11-18 ka). The glacial termination period was highly transient, with atmospheric CO₂ varying by ~85 ppm in <10 kyr, and large changes in carbon isotopes. Thus it is anticipated that in a model-data reconstruction, model parameters would vary substantially for this period. Our strategy of integrating the model forward to an equilibrium state for each MIS as intervals of discrete climate and CO₂, would be unsuitable when applied to the last glacial termination.

2.2.1 Model forcings and parameter variations

We took a reconstructed SST time series for the last 130 kyr (Kohfeld and Chase, 2017), mapped these to SCP-M's surface boxes, and averaged the time series across each MIS (Fig. 2(A)). We have extrapolated an Antarctic sea ice cover proxy as shown in Fig. 2(B) (Wolff et al., 2010) to the profiles for sea surface salinity (Fig. 2(C)) and the polar Southern Ocean air-sea gas exchange parameter (Fig. 2(D)). For example, our notional reduction in the strength of the polar Southern Ocean air-sea gas exchange due to Antarctic sea ice cover (-30%) is linearly (negatively) profiled with the Antarctic sea ice proxy time series of Wolff et al. (2010). We also vary the North Atlantic air-sea gas exchange parameter to the same extent (-30%) to approximate the effects of increased sea ice during MIS 2 and MIS 4 (Hoff et al., 2015; Maffezzoli et al., 2018).

Adkins et al. (2002) reconstructed LGM deep-sea salinity for the Southern, Atlantic and Pacific Oceans. They found increased salinity for the LGM at all locations, across a range of +0.95-2.4 practical salinity units (psu) above modern values, with an average value of +1.5 psu. The most saline LGM waters were in the Southern Ocean (+ 2.4 psu), with Atlantic and Pacific waters ranging +0.95-1.46 psu and an average of +1.2 psu. Adkins et al. (2002) also observed that within a (globally) more saline ocean, lower glacial temperatures would have caused less evaporation during the LGM, a negative feedback on salinity. We chose a global forcing for LGM sea surface salinity of +1 psu for the global ocean, and +2 psu for the polar South-

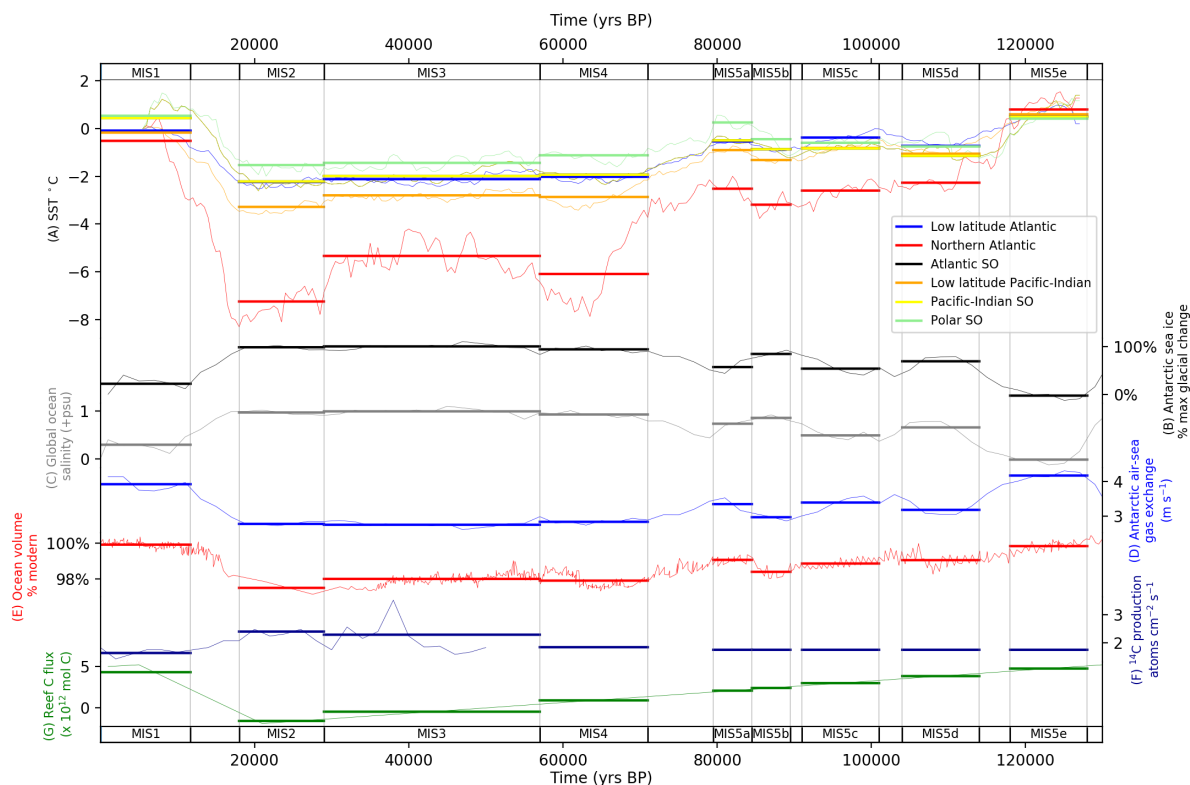


Figure 2. Model forcings for MIS across the last glacial cycle. (A) sea surface temperature reconstruction of (Kohfeld and Chase, 2017), mean values mapped into SCP-M surface boxes (fine lines) and averaged across MIS (bold lines). (B) Proxy for Antarctic sea ice extent using ssNa fluxes from the EPICA Dome C ice core (Wolff et al., 2010), used to temporally contour MIS model forcings for (C) salinity (Adkins et al., 2002) and (D) polar Southern Ocean air-sea gas exchange. Global ocean salinity is forced to a glacial maximum of +1 psu (shown in (C)) and the polar Southern Ocean is forced to +2 psu (not shown), as modified from Adkins et al. (2002). Ocean volume (E) forced using global relative sea level reconstruction of Rohling et al. (2009). (F) Atmospheric ^{14}C production rate time series for 0-50 ka of Muscheler et al. (2014). Long-term values assumed for >50 ka (Key, 2001). (G) Shallow water carbonate flux of carbon from Ridgeway et al. (2003) profiled across the glacial cycle using a curve from Opdyke and Walker (1992). Fine lines are the time series data and bold lines are the model forcings in each MIS. Data behind the figure are shown in Supplementary Information.

ern Ocean, relative to the interglacial period. These values conservatively reflect the hypothesis that surface evaporation may have been less in the LGM, hence a lesser magnitude of change in salinity in the surface ocean relative to the deep ocean values estimated by Adkins et al. (2002), and also that the most voluminous parts of the ocean were less saline than the Southern Ocean (Adkins et al., 2002). In our model-data experiments, the estimated glacial change in sea surface salinity (Fig. 2(C)), is also contoured through time with the variation in Antarctic sea ice cover of Wolff et al. (2010). Adkins et al. (2002) observed that glacial salinity is a poor predictor of global mean sea level, due to storage of saline waters in ice shelves and groundwater



reserves, hence the proxy for Antarctic sea ice cover may have a more direct linkage to sea surface salinity than using global sea level, for our purposes of estimating temporal evolution in salinity.

Rohling et al. (2009) reconstructed global relative sea level (RSL) over the past five glacial cycles. According to Rohling et al. (2009), the glacial RSL minimum was \sim -115m at \sim 27 ka, immediately prior to the LGM. We perform a simple calculation to reduce ocean depth and volume in SCP-M, in line with the Rohling et al. (2009) time series. In a box model this is only an approximation, given the lack of topographical detail. Varying ocean box volume and surface area, effects the ocean surface area available for in-gassing and de-gassing, and overall ocean capacity to store CO_2 , which impacts atmospheric CO_2 , $\delta^{13}\text{C}$ and $\Delta^{14}\text{C}$ (O'Neill et al., 2019). Opdyke and Walker (1992) reconstructed coral reef carbonate fluxes of CaCO_3 for the last glacial cycle, for the purposes of modelling the "coral reef hypothesis". According to Opdyke and Walker (1992), reef carbon fluxes (out of the ocean) declined through the glacial cycle, with net dissolution in MIS 2 and MIS 3 leading to positive fluxes of carbon and alkalinity into the ocean in those periods. Fluxes of carbon and alkalinity out of the ocean into coral reefs, rebounded from the LGM (MIS 2) into the Holocene (MIS 1), driven by increased sea level and temperature (Kleypas, 1997). Given that Opdyke and Walker (1992) evaluated the possibility for coral reefs to drive the entire glacial-interglacial CO_2 variation, we have taken the more conservative modelling assumption of Ridgeway et al. (2003) of 0.5×10^{17} mol C, for postglacial accumulation of coral reefs. We have profiled this value across the glacial cycle accumulation/dissolution curve of Opdyke and Walker (1992), as shown in Fig. 2. We applied the estimated atmospheric production rate for ^{14}C for the last 50 kyr of Muscheler et al. (2014), with a long term average production rate of ~ 1.7 atoms $\text{cm}^{-2} \text{s}^{-1}$ assumed for 50-130 ka (Key, 2001).

The terrestrial biosphere module in SCP-M does not explicitly represent the large glacial "inert" carbon pool in permafrost and tundra (e.g. Ciais et al., 2012). These vegetation types may significantly imprint the glacial cycle terrestrial biosphere CO_2 and $\delta^{13}\text{C}$ signatures (Ciais et al., 2012; Hoogakker et al., 2016; Eggleston et al., 2016). Eggleston et al. (2016) observed a permanent increase in atmospheric $\delta^{13}\text{C}$ during the last glacial cycle, of $\sim 0.5\%$, and attributed its likely cause to glacial growth in tundra. As a crude measure to account for the counter- CO_2 cycle growth in tundra in the LGM, we force the 'pre-carbon fertilisation' terrestrial biosphere parameter in SCP-M in the range $\sim +4$ -10 PgC yr^{-1} , increasing into the LGM (MIS 2), and maintained in the Holocene (MIS 1). It is appropriate to maintain the forcing in the Holocene, as the posited effects of tundra growth on atmospheric $\delta^{13}\text{C}$ during the lead-up and into the LGM, are not reversed after the termination (Eggleston et al., 2016). SCP-M calculates net primary productivity (NPP) using this input, as a function of carbon fertilisation (Harman et al., 2011).

$\sim 5,000$ model simulations were undertaken across the parameter ranges in Table 1 for each MIS. Parameters were varied simultaneously to allow coverage of all possible combinations of the parameter values within their respective experiment ranges. Within these ranges, values are incremented by 1 Sv for GOC (Ψ_1) and AMOC (Ψ_2), and ~ 0.5 mol C $\text{m}^{-2} \text{yr}^{-1}$ for Atlantic Southern Ocean biological export productivity (Z). Each simulation was run for 10 kyr to enable the model to achieve steady state. We show the experiment ranges for the biological export productivity parameter Z for the Atlantic and Pacific-Indian sectors of the Southern Ocean (Table 1). In SCP-M, the Pacific-Indian Southern Ocean biological export productivity parameter (in mol C $\text{m}^{-2} \text{yr}^{-1}$) is set by default at a value of $\sim 40\%$ of the corresponding Atlantic sector Southern Ocean box,



Table 1. Free-floating parameter ranges in the model-data experiments, for global overturning circulation (Ψ_1), Atlantic meridional overturning circulation (Ψ_2) and Southern Ocean biological export productivity (Z). Parameters were varied simultaneously across these ranges and then optimised against proxy data in each MIS. Also shown are MIS time slices as per Lisiecki and Raymo (2005), with a slight modification to MIS 1 and 2 to exclude the transient glacial termination. The Pacific-Indian Southern Ocean biology parameter is set at a base value of $\sim 40\%$ Atlantic Southern Ocean box, but scales linearly with the Atlantic Ocean parameter in the experiments. The smaller values for Pacific-Indian Southern Ocean takes account of natural observations of a relatively stronger biological export productivity in the Atlantic sector of the subpolar Southern Ocean (e.g. Dunne et al., 2005; Sarmiento and Gruber, 2006; Henson et al., 2011; Siegel et al., 2014; DeVries and Weber, 2017).

MIS	Time (ka)	GOC (Ψ_1) Sv	AMOC (Ψ_2) Sv	Southern Atlantic (Pacific-Indian) Ocean biology (Z) $\text{mol C m}^{-2} \text{ yr}^{-1}$
~ 1	0-11.7	10-35	10-25	0.5-6.5 (0.2-3.0)
~ 2	18-29	10-35	10-25	0.5-6.5 (0.2-3.0)
3	29-57	10-35	10-25	0.5-6.5 (0.2-3.0)
4	57-71	10-35	10-25	0.5-6.5 (0.2-3.0)
5a	79.5-84.5	10-35	10-25	0.5-6.5 (0.2-3.0)
5b	84.5-89.5	10-35	10-25	0.5-6.5 (0.2-3.0)
5c	91-101	10-35	10-25	0.5-6.5 (0.2-3.0)
5d	104-114	10-35	10-25	0.5-6.5 (0.2-3.0)
5e	118-128	10-35	10-25	0.5-6.5 (0.2-3.0)

to align with natural observations of variations in the Southern Ocean biological export productivity (e.g. Dunne et al., 2005; Sarmiento and Gruber, 2006; Henson et al., 2011; Siegel et al., 2014; DeVries and Weber, 2017). This variation is reflected in the values in Table 1. In the experiments, the values for Z in the Pacific-Indian Southern Ocean surface box scale linearly with the values for the Atlantic Southern Ocean surface box (Table 1). Herein we focus our presentation and discussion of the experiment results for the Z parameter on the Atlantic Southern Ocean, due to its prominence in glacial cycle hypotheses for increased biological productivity (e.g. Martinez-Garcia et al., 2014; Lambert et al., 2015; Muglia et al., 2018).

2.2.2 Optimisation procedure

We performed a least squares optimisation of the model experiment output against MIS data for atmospheric CO_2 , atmospheric and deep and abyssal ocean $\Delta^{14}\text{C}$ and $\delta^{13}\text{C}$, and deep and abyssal ocean carbonate ion proxy, to source the best-fit parameter



Table 2. Ocean and atmosphere proxy data sources for the last glacial cycle

Indicator	Time period coverage	Reference
Atmosphere CO ₂	0-800 ka	Bereiter et al. (2015)
Atmosphere δ ¹³ C	0-155 ka	Eggleston et al. (2016)
Atmosphere Δ ¹⁴ C	0-50 ka	Reimer et al. (2009)
Ocean δ ¹³ C	0-120 ka	Oliver et al. (2010)
Ocean Δ ¹⁴ C	0-40 ka	Skinner and Shackleton (2004), Marchitto et al. (2007), Barker et al. (2010), Bryan et al. (2010), Skinner et al. (2010), Burke and Robinson (2012), Davies-Walczak et al. (2014), Skinner et al. (2015), Chen et al. (2015), Hines et al. (2015), Sikes et al. (2016), Ronge et al. (2016), Skinner et al. (2017), Zhao et al. (2017)
Ocean carbonate ion proxy	0-705 ka	Yu et al. (2010), Yu et al. (2013), Yu et al. (2014b), Yu et al. (2014a), Broecker et al. (2015), Yu et al. (2016), Qin et al. (2017), Qin et al. (2018), Chalk et al. (2019)

values for GOC, AMOC and Southern Ocean biological productivity in each time slice - a brute force form of the *gradient descent* method for optimisation (e.g. Strutz, 2016). The equation for least fit applied was:

$$Opt_n = Min \sum_{i,k=1}^N \left(\frac{R_{i,k} - D_{i,k}}{\sigma_{i,k}} \right)^2 \quad (2)$$

where: Opt_n = optimal value of parameters n (e.g. GOC, AMOC and Southern Ocean biological productivity), $R_{i,k}$ = model output for concentration of each element i in box k , $D_{i,k}$ = average data concentration each element i in box k and $\sigma_{i,k}$ = standard deviation of the data for each element i in box k . The standard deviation performs two roles. It normalises for different unit scales (e.g. ppm, ‰ and $\mu\text{mol kg}^{-1}$), which allows multiple proxies to be incorporated in the optimisation, and reduces the weighting of a proxy data point with a high standard deviation, and therefore an uncertain value. The weighting by proxy data standard deviation also fulfils the important role of accounting for data variance in the optimised parameter results, such that the effects of data variance are embedded in the optimised parameter values. Where proxy data is unavailable for a box, that data and box combination is automatically omitted from the optimisation routine. The experiment routine returns the model run with the best fit to the data, and the model's parameters and results.



2.3 Data

The model-data optimisation rests on compilations of atmospheric and ocean paleo proxy data. We compile and apply published proxy data for atmospheric CO_2 , $\delta^{13}\text{C}$ and $\Delta^{14}\text{C}$ and ocean $\delta^{13}\text{C}$, $\Delta^{14}\text{C}$ and carbonate ion. Sources of proxy data are shown in Table 2 and data locations in Fig. 3.

5 2.3.1 Ocean carbon isotopes

We gathered published marine $\Delta^{14}\text{C}$ data extending back to ~ 40 ka (Table 2). Our dataset incorporates individual records contributed over the last \sim thirty years and supplemented by the recent compilations of Skinner et al. (2017) and Zhao et al. (2017). The data total ~ 75 individual location estimates for benthic and planktonic foraminifera, and deep sea corals. We have restricted our efforts to time series which contain independent calendar ages, and therefore corrections for radioactive decay in the time since the sample was deposited (yielding $\Delta^{14}\text{C}$). Figure 3 shows the geographic distribution of the $\Delta^{14}\text{C}$ data, which is generally concentrated on ocean basin margins. Some regions, such as the central Pacific, southern Indian and polar Southern Ocean, are devoid of data.

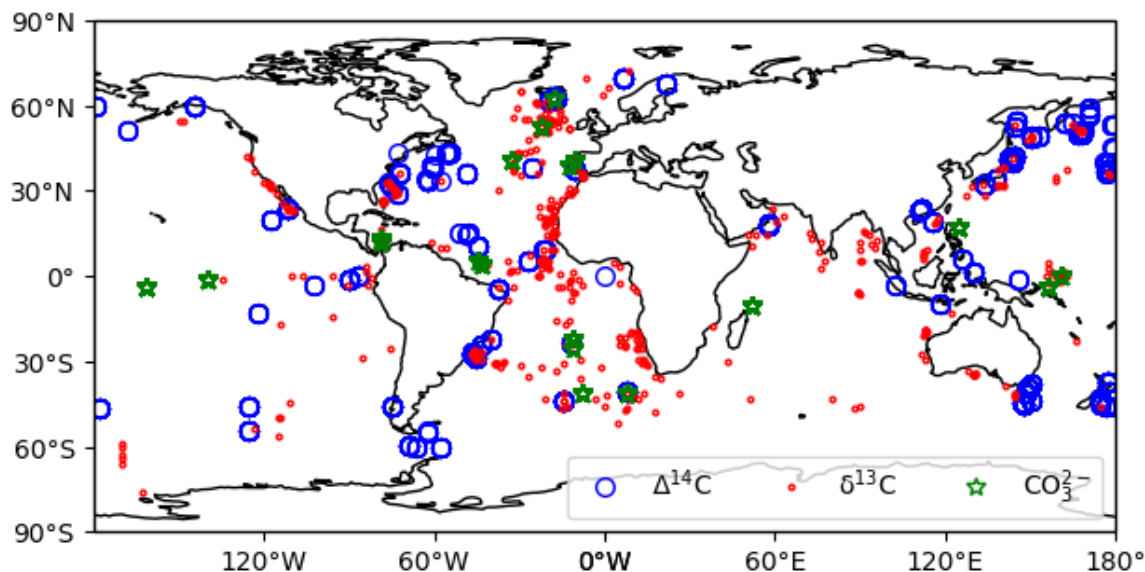


Figure 3. $\Delta^{14}\text{C}$, $\delta^{13}\text{C}$ and CO_3^{2-} data locations. $\Delta^{14}\text{C}$ and CO_3^{2-} data was compiled from published estimates. For $\delta^{13}\text{C}$ we take the compilation of Oliver et al. (2010).

Oliver et al. (2010) compiled a global dataset of 240 cores of marine $\delta^{13}\text{C}$ data encompassing benthic and planktonic species over the last ~ 150 kyrs. Oliver et al. (2010) observed considerable uncertainties associated with the broad range of species included, particularly for the planktonic foraminifera. By comparison, Peterson et al. (2014) aggregated marine $\delta^{13}\text{C}$ for the LGM and late Holocene periods, as time period averages, exclusively sampling the benthic *C. wuellerstorfi* data, which is



a more reliable indicator of marine $\delta^{13}\text{C}$ (Oliver et al., 2010; Peterson et al., 2014). To narrow the range of uncertainty, we constrain our use of marine $\delta^{13}\text{C}$ data to the deep and abyssal benthic foraminifera samples in the Oliver et al. (2010) dataset. Figure 3 shows the $\delta^{13}\text{C}$ data locations from Oliver et al. (2010), which are concentrated in the Atlantic Ocean. We mapped and averaged the carbon isotope data into SCP-M's boxes on depth and latitude coordinates (Fig. 1), and averaged for each 5 MIS time slice.

2.3.2 Carbonate ion proxy

We aggregated ocean carbonate ion proxy data from the sources shown in Table 2 and locations in Fig. 3, mapped into SCP-M box coordinates and averaged the data across MIS. The data coverage for CO_3^{2-} is relatively sparse, with <20 individual site locations across the global ocean. However, the depth and lateral coverage of SCP-M's boxes is large, particularly in the case of the deep ocean boxes, which cover the full lateral extent of the Pacific-Indian and Atlantic oceans, and depth ranges of 100-2,500m (Pacific-Indian) and 250-2,500m (Atlantic). CO_3^{2-} can vary by more than $100 \mu\text{mol kg}^{-1}$ across the depth range 100-2,500m, and can vary by up to $\sim 200 \mu\text{mol kg}^{-1}$ in the shallow ocean (e.g. Sarmiento and Gruber, 2006; Yu et al., 2014b, a). Some boxes contain only one core, creating an exceptionally low standard deviation range relative to the other proxies. In other cases, such as the deep Atlantic ocean, the data points are clustered within the 2,000-2,500m depth range, the bottom third of the corresponding SCP-M box. This clustering becomes a problem for the SCP-M box model, which outputs average concentrations over the complete depth range of each box - a drawback of using a large resolution box model to analyse proxy data at a global ocean level. Furthermore, the very low standard deviations associated with the CO_3^{2-} data (data shown in Supplementary Information) cause it to assume a disproportionate weighting in the model-data optimisation, which uses standard deviation for weighting of proxies, relative to ocean $\delta^{13}\text{C}$ and $\Delta^{14}\text{C}$. The latter proxies often have box standard deviations up to 100% of their mean value, when averaged across a box. This issue is also an artefact of our procedure necessary to normalise the different proxies (each in unique units) in a multi-proxy model-data optimisation, by using the standard deviation as a weighting. To deal with this, we have assigned an arbitrary standard deviation (weighting) of $50 \mu\text{mol kg}^{-1}$ to CO_3^{2-} data observations, which acts as a feasible weighting for the processing of the CO_3^{2-} data, and of a similar proportion to other proxy data, in our model-data optimisation. This value is approximately half the variation in CO_3^{2-} observed over the depth range 100-2,500m in the modern ocean (e.g. Key et al., 2004; Yu et al., 2014b).

3 Data analysis

Figure 4 shows the atmospheric data used to constrain the model, mapped into MIS time slices. There are three major reductions in atmospheric CO_2 in the lead-up to the LGM (Fig. 4(A)). A drop of ~ 25 ppm in MIS 5d, a further drop of ~ 30 ppm in MIS 4, and finally a fall of ~ 20 ppm in the period leading up to the LGM (between MIS 2 and 4). These are the three major CO_2 events described in Kohfeld and Chase (2017), and, combined with additional reductions of ~ 10 ppm throughout the period, yield a total drop of ~ 85 ppm from the penultimate interglacial to the LGM. There is also a transient drop in atmospheric CO_2 , of 14 ppm, at MIS 5b. CO_2 increases by ~ 85 ppm in the glacial termination and Holocene periods.



Atmospheric $\delta^{13}\text{C}$ (Fig. 4(B)) increases by $\sim 0.5\%$ between the penultimate interglacial (MIS 5e) and the Holocene, with temporary falls at MIS 5d, MIS 4, MIS 3 and in the last glacial termination (between MIS 1 and 2). The increase in $\delta^{13}\text{C}$ across the glacial cycle, is attributed to the growth of tundra at high latitudes (e.g. Ciais et al., 2012; Eggleston et al., 2016; Hoogakker et al., 2016). The large drop in $\delta^{13}\text{C}$ in MIS 4 accompanies a ~ 30 ppm fall in CO_2 . The drop in $\delta^{13}\text{C}$ is likely
5 caused by a reduction in the terrestrial biosphere, itself driven by the fall in CO_2 (Hoogakker et al., 2016). The reduction in atmospheric $\delta^{13}\text{C}$ at the last glacial termination, coincident with atmospheric CO_2 increase, is attributed to the release of deep-ocean carbon to the atmosphere as a result of increased ocean circulation (Schmitt et al., 2012). The subsequent rebound of $\delta^{13}\text{C}$ in the termination period and the Holocene is believed to result from terrestrial biosphere regrowth, in response to increased CO_2 and carbon fertilisation (Schmitt et al., 2012; Hoogakker et al., 2016).

10 The atmospheric $\Delta^{14}\text{C}$ data covers the period 0-50ka (Reimer et al., 2009). During this period, $\Delta^{14}\text{C}$ is heavily influenced by declining atmospheric ^{14}C production (Broecker and Barker, 2007; Muscheler et al., 2014). In addition, an acceleration in $\Delta^{14}\text{C}$ decline at the last glacial termination is attributed to the release of old, ^{14}C -depleted waters from the deep ocean, due to increased GOC and/or AMOC (Sikes et al., 2000; Marchitto et al., 2007; Skinner et al., 2010; Burke and Robinson, 2012; Skinner et al., 2017).

15 Figure 5 shows deep and abyssal ocean $\delta^{13}\text{C}$ data mapped into SCP-M box model space and averaged across MIS. The visual offset between deep and abyssal proxy data values is regularly interpreted as an indicator of the strength of deep ocean circulation and/or mixing, or biological productivity, during the LGM and the Holocene (e.g. Sikes et al., 2000; Curry and Oppo, 2005; Marchitto et al., 2007; Oliver et al., 2010; Skinner et al., 2010; Burke and Robinson, 2012; Yu et al., 2013, 2014a; Skinner et al., 2015, 2017). The deep-abyssal Atlantic $\delta^{13}\text{C}$ time series (Fig. 5(A)) exhibits modest widening in the deep and
20 abyssal offset between MIS 5d and 5e, again at MIS 5b, and a further widening at MIS 4 and at MIS 2 (the LGM). The widening of the offset during MIS 2-4 is caused primarily by more negative abyssal $\delta^{13}\text{C}$ values. The offset is almost closed in MIS 1 (the Holocene). The deep Atlantic $\delta^{13}\text{C}$ range itself also widens considerably from MIS 4, and narrows after the LGM. Oliver et al. (2010) and Kohfeld and Chase (2017) interpreted these patterns as the result of weakened deep Atlantic ocean circulation at MIS 4 and at the LGM, rebounding in the post glacial period.

25 The Pacific-Indian $\delta^{13}\text{C}$ data (Fig. 5(B)) shows a drop in abyssal $\delta^{13}\text{C}$ and modest widening in the deep-abyssal offset at MIS 5d, continuing to MIS 5a. Importantly, the more negative abyssal $\delta^{13}\text{C}$ values during MIS 5a-5d, occur at the same time that atmospheric $\delta^{13}\text{C}$ becomes more positive (Fig. 4(B)), suggesting that the abyssal Pacific-Indian ocean became more isolated from the atmosphere during this period. This is qualitative evidence for slowing ocean circulation or increased biological export productivity in the Pacific-Indian ocean, at that time. This also corresponds with a ~ 35 ppm fall in CO_2 across MIS 5a-5e (Fig.
30 4(A)). Abyssal Pacific-Indian $\delta^{13}\text{C}$ drops further at MIS 4, and again at the LGM, and then rebounds from the LGM into the Holocene period, as also observed in the Atlantic Ocean $\delta^{13}\text{C}$ data.

Ocean $\Delta^{14}\text{C}$ data covers the MIS 1-3 periods, and the LGM and Holocene in most detail (Fig. 6). We show ocean $\Delta\Delta^{14}\text{C}$, which is atmospheric less ocean $\Delta^{14}\text{C}$. This calculation is made in attempt to normalise the effects of varying atmospheric ^{14}C production through the glacial cycle (Broecker and Barker, 2007; Muscheler et al., 2014), which imparts a dominant influence
35 on the ocean $\Delta^{14}\text{C}$ trajectory. Given the sparse data coverage for MIS 3, we focus our analysis on MIS 1 and 2. The $\Delta\Delta^{14}\text{C}$

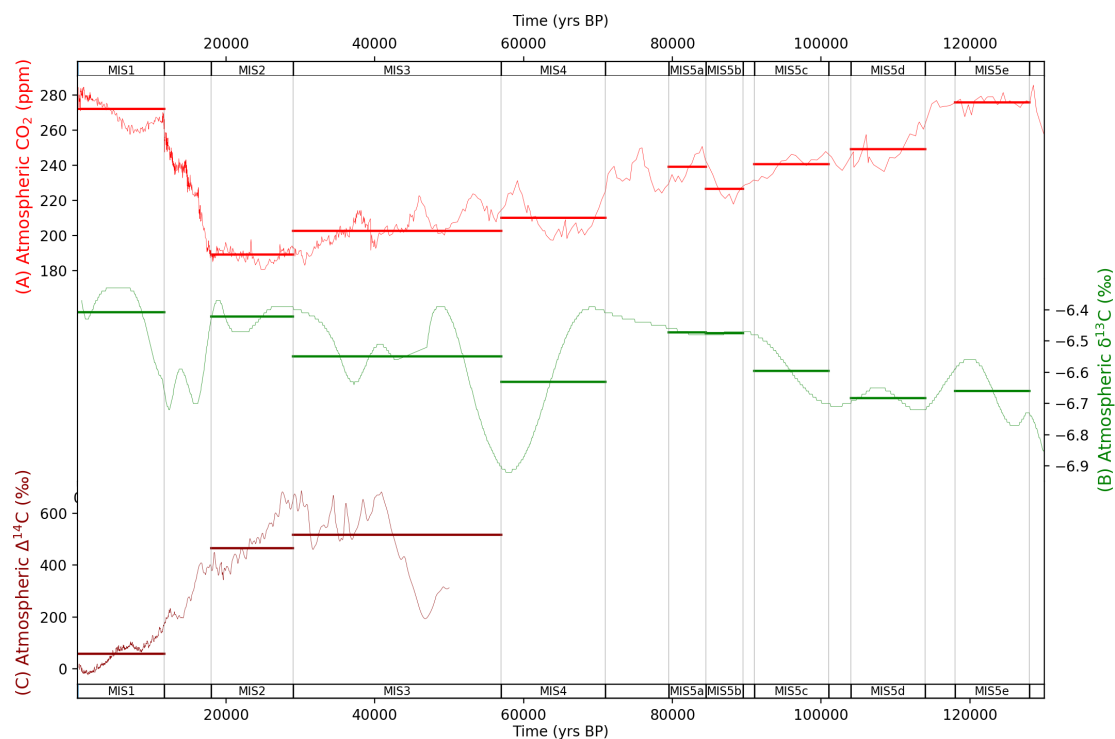


Figure 4. MIS atmosphere data for (A) atmospheric CO₂ (Bereiter et al., 2015), (B) δ¹³C (Eggleston et al., 2016) and (C) Δ¹⁴C (Reimer et al., 2009). Data are shown in fine lines, with bold horizontal lines for MIS-sliced data. Natural observations for Δ¹⁴C do not exist beyond ~50 ka due to the radioactive decay of ¹⁴C. Data behind the figure are shown in Supplementary Information.

time series exhibits two key features across the LGM (MIS 2) and Holocene periods (MIS 1). First, there is a narrowing in the spread of values between the shallow and abyssal ocean from the LGM to the Holocene, in both the Atlantic (Fig. 6(A)) and Pacific-Indian (B) basins. Second, all ocean boxes display an increase in ΔΔ¹⁴C from the LGM to the Holocene, towards equilibrium with the atmosphere. These patterns are believed to represent increased overturning circulation in the Atlantic and Pacific-Indian basins across the LGM-Holocene. Increased ocean overturning brought old, Δ¹⁴C-negative water up from the deep and abyssal oceans, mixing with shallow and intermediate waters, and eventually into contact with the atmosphere, where ¹⁴C is produced - known as "increased ventilation" (e.g. Sikes et al., 2000; Marchitto et al., 2007; Bryan et al., 2010; Skinner et al., 2010; Burke and Robinson, 2012; Davies-Walczak et al., 2014; Skinner et al., 2014; Hines et al., 2015; Freeman et al., 2016; Sikes et al., 2016; Skinner et al., 2017).

10 The Atlantic ocean CO₃²⁻ time series shows a similar pattern to ΔΔ¹⁴C and δ¹³C, with a wide dispersion of shallow-abyssal and deep-abyssal concentrations at the LGM, which narrows at the Holocene (Fig. 6). This pattern has been interpreted as varying strength and/or depth of AMOC and biological productivity in the Atlantic Ocean (e.g. Yu et al., 2013, 2014b, a, 2016). The abyssal Atlantic CO₃²⁻ pattern, which spans the last glacial cycle, is punctuated by two downward excursions (Fig.

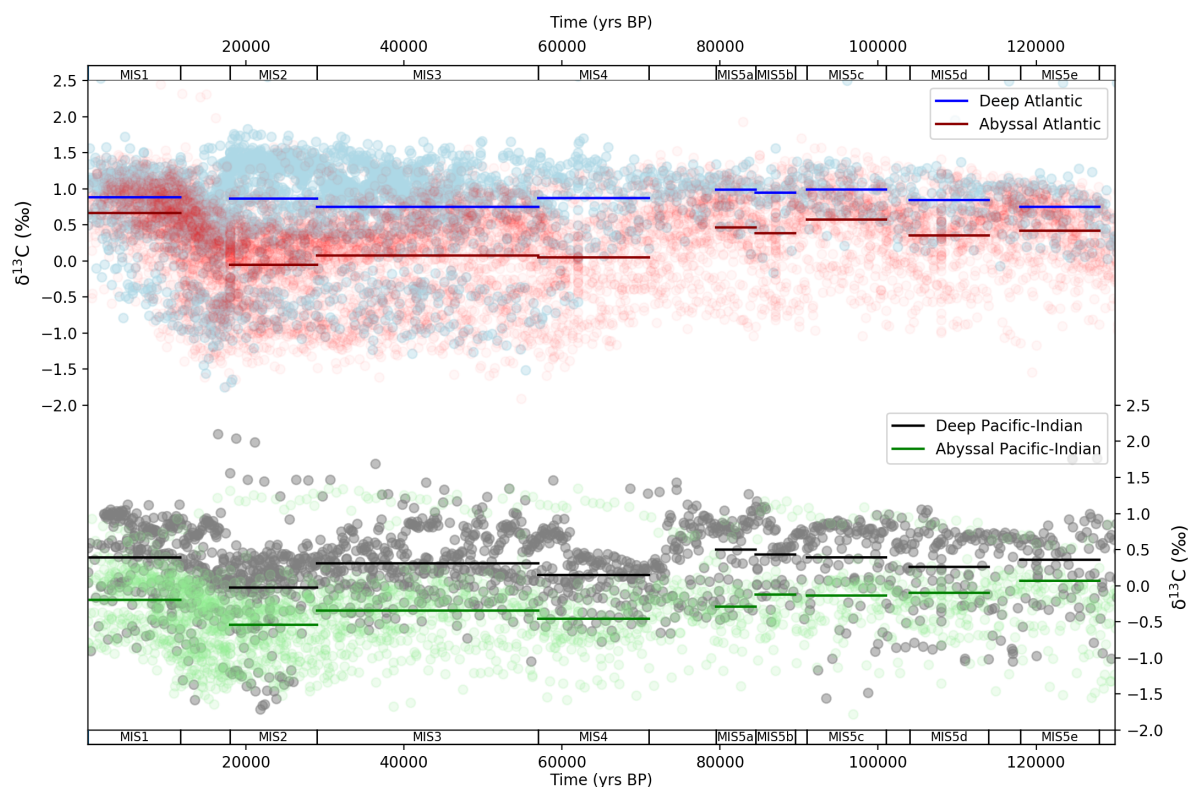


Figure 5. MIS ocean data mapped into SCP-M box model dimensions for $\delta^{13}\text{C}$ (Oliver et al., 2010). Data (round circles) are mapped into model boxes and averaged across MIS slices (bold lines). Sources listed in Table 2. Data behind the figure are shown in Supplementary Information.

- 6). These occur at MIS 4 and MIS 2, corresponding to the second major atmospheric CO_2 drop in the glacial cycle, and the LGM, respectively. The lower CO_3^{2-} value at MIS 4 was interpreted by Yu et al. (2016) as shoaling of AMOC and increased carbon storage in the deep-abyssal Atlantic Ocean. This signal is repeated at the LGM, where further shoaling and slowing AMOC is believed to have contributed to deep oceanic drawdown of CO_2 from the atmosphere (Yu et al., 2013, 2014b, a).
- 5 There is a transient drop in abyssal Atlantic ocean CO_3^{2-} at MIS 5b, which coincides with a transient drop in abyssal Atlantic ocean $\delta^{13}\text{C}$ and atmospheric CO_2 (-14 ppm), suggesting a common link.

The Pacific Ocean is thought to partially buffer the effects of ocean circulation on CO_3^{2-} concentrations via changes in shallow (reef) and deep carbonate production and dissolution, and therefore displays less variation across the MIS (Yu et al., 2014b; Qin et al., 2017, 2018). The deep and abyssal Pacific-Indian ocean data shows a persistent trend of increasing CO_3^{2-} through the glacial cycle, suggesting that it is influenced by variations in shallow and deep sea carbonate production and dissolution, rather than by deep ocean circulation (Yu et al., 2014b; Qin et al., 2017, 2018). Notable exceptions are MIS 5d and MIS 4. At MIS 5d, both deep and abyssal Pacific-Indian ocean CO_3^{2-} drop, aligning with the contemporary drop in abyssal

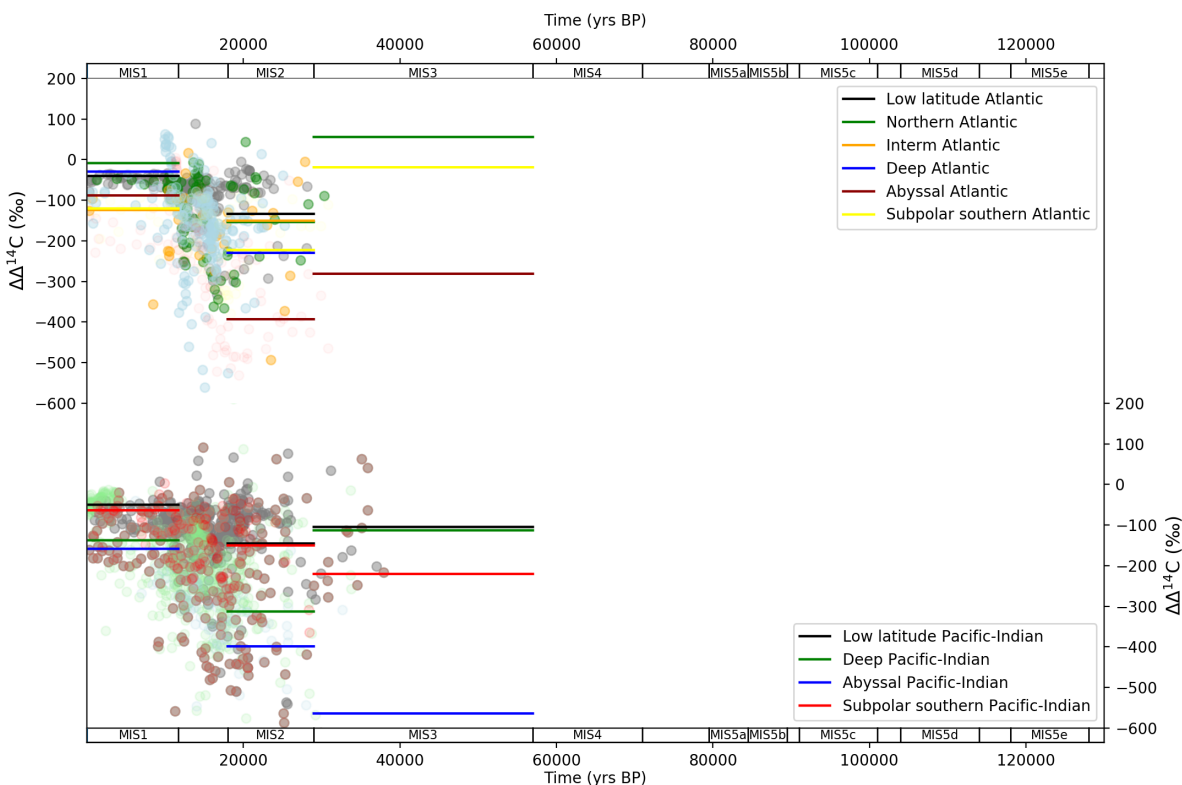


Figure 6. MIS stage ocean data mapped into box model dimensions for $\Delta\Delta^{14}\text{C}$. Data (round circles) are mapped into model boxes and averaged across MIS slices (bold lines). Sources listed in Table 2. Natural observations do not exist beyond ~ 50 ka due to the radioactive decay of ^{14}C . Data behind the figure are shown in Supplementary Information.

$\delta^{13}\text{C}$ and atmospheric CO_2 (Fig. 5(B)), suggesting a possible common driver, and providing additional qualitative evidence for changes in either Pacific-Indian ocean circulation or biology, at this time. At MIS 4, there is a drop in deep Pacific-Indian CO_3^{2-} and a modest widening in the deep-abyssal offset from prior periods, also suggestive of the influence of deep ocean circulation and/or biological export productivity. The widest Pacific-Indian deep-abyssal offset CO_3^{2-} is observed in MIS 3, also seen in the $\delta^{13}\text{C}$ and $\Delta\Delta^{14}\text{C}$ data, indicating it is a persistent feature of the proxy records, and suggesting MIS 3 may be the nadir of Pacific-Indian ocean circulation and/or the peak in biological activity in the glacial cycle, and at least that most changes in this part of the ocean took place prior to the LGM.

4 Results

Figure 8 shows the data-optimised values returned from the model-data experiments for GOC, AMOC and Atlantic Southern Ocean biological productivity parameters, in each MIS ("X" symbols). The optimised values take account of data variance,

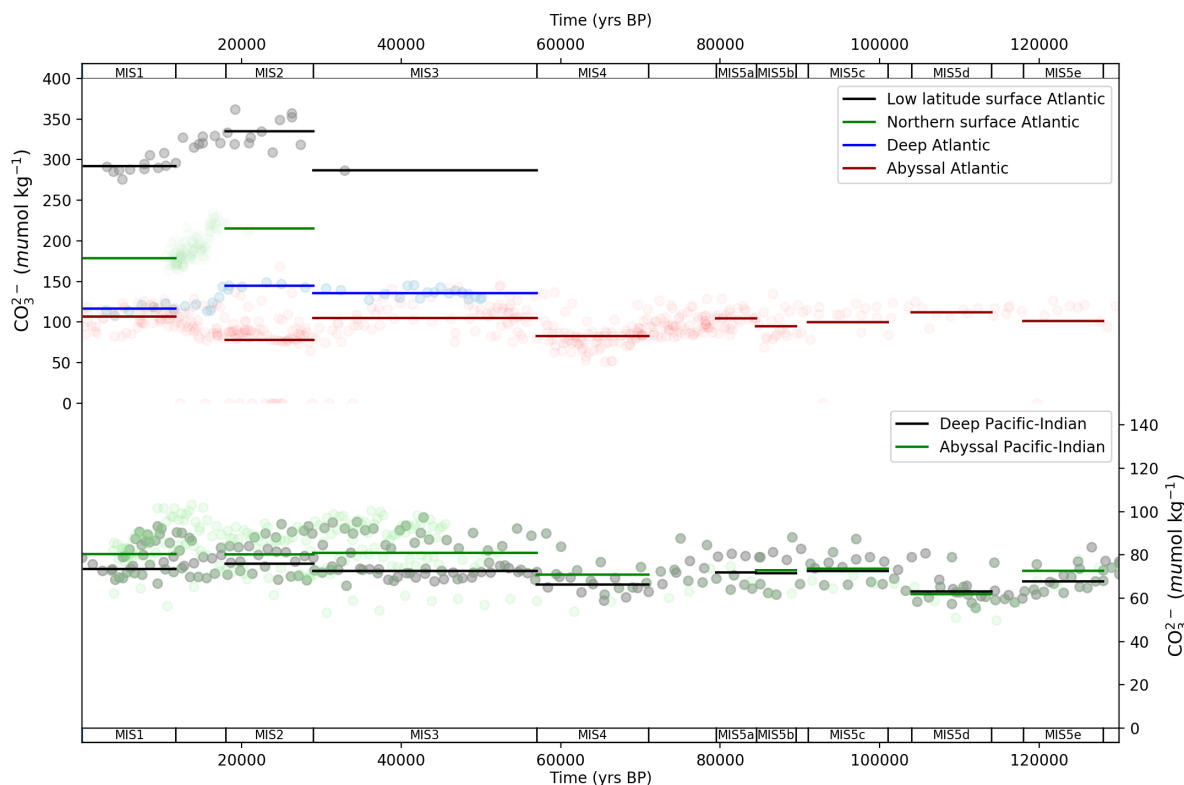


Figure 7. MIS stage ocean data mapped into box model dimensions for carbonate ion proxy. Data (round circles) are mapped into model boxes and averaged across MIS slices (bold lines). Sources listed in Table 2. Data behind the figure are shown in Supplementary Information.

due to the weighting of proxy data points by their standard deviation in the model-data optimisation equation (Eq. 2). The full range of model-data experiment results are shown in the Supplementary Information. The GOC parameter (Ψ_1) value falls from 28 Sv to 19 Sv between MIS 5d and 5e, with gradual declines during MIS 5b-5c, followed by stabilisation at MIS 4-5a, and a further drop at MIS 3. It remains steady at the LGM, just above its minimum glacial value at MIS 3, and then increases to 26 Sv in MIS 1. AMOC (Ψ_2) remains largely unchanged across the period MIS 5a-5e, with a transient drop at MIS 5b. A pronounced fall (-6 Sv) takes place in MIS 4, maintained until the LGM, with a transient increase at MIS 3, before increasing to 20 Sv in MIS 1. Importantly, Ψ_2 closely follows the abyssal Atlantic $\delta^{13}\text{C}$ and CO_3^{2-} data pattern across the glacial cycle, and $\Delta\Delta^{14}\text{C}$ from the LGM to the Holocene (Figs 5-7). Ψ_2 remains elevated during MIS 5c and 5d, increasingly slightly, before dropping temporarily in MIS 5b (abyssal Atlantic $\delta^{13}\text{C}$ and CO_3^{2-} , and atmospheric CO_2 , also drop at this point), before rebounding at MIS 5a and then falling synchronously with abyssal Atlantic $\delta^{13}\text{C}$ and CO_3^{2-} concentrations during MIS 4 and MIS 2. Southern Ocean biological export productivity (Z) drops early in the glacial cycle (MIS 5d), then steadily increases during MIS 4 and MIS 3. Atlantic (Pacific-Indian) Southern Ocean Z spikes to 6 (2) $\text{mol C m}^{-2} \text{ yr}^{-1}$ in the LGM, then falls



to 2.3 (0.8) mol C m⁻² yr⁻¹ in MIS 1. The value for Z at MIS 4 is the same as for MIS 5e, however is 1.3 mol C m⁻² yr⁻¹ higher than MIS 1, indicating elevated values for Z in MIS 4 when compared with the Holocene.

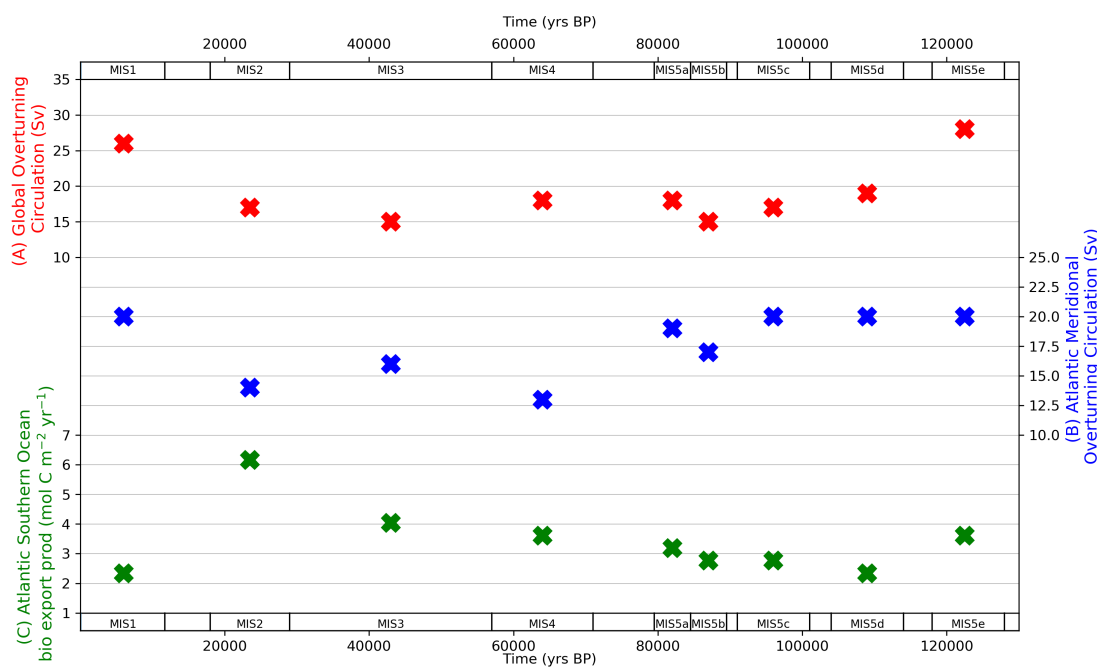


Figure 8. Model-data experiment results for global overturning circulation (A), Atlantic meridional overturning circulation (B) and Atlantic Southern Ocean biological export productivity (C). "X" symbols mark the optimal parameter values returned from the model-data experiments. The optimised values take account of data variance, due to the weighting of proxy data points by their standard deviation in the model-data optimisation equation (Eq. 2). Data for optimised parameter values shown in the figure are contained in Supplementary Information.

Figure 9 show the optimised model-data output for atmospheric CO₂ and ocean carbonate ion proxy, compared with the data observations, in each MIS. This shows how well the model is constrained by the proxy data, and also how well the model-data output of parameter values can explain the proxy data patterns as described in the data analysis section. The model-data results fall within one standard deviation of atmospheric CO₂ and deep and abyssal CO₃²⁻ data, and mostly on the MIS means, across the MIS periods. The results for the deep Pacific-Indian box CO₃²⁻ fall near the top of the standard deviation of the data, which we have notionally set at 50 μmol kg⁻¹ due to the sparse coverage of data, clustering of the data near the bottom of that box and low standard deviation ranges around the box mean. The combined effect increases the difficulty of data-matching across all of the proxies, hence our adoption of the default standard deviation of 50 μmol kg⁻¹ to allow sufficient tolerance and an



appropriate weighting of the CO_3^{2-} data, relative to ocean $\delta^{13}\text{C}$ and $\Delta^{14}\text{C}$, in the model-data optimisation. This issue could be resolved with a higher resolution model, more data, and/or a more complex treatment of CO_3^{2-} variation with depth.

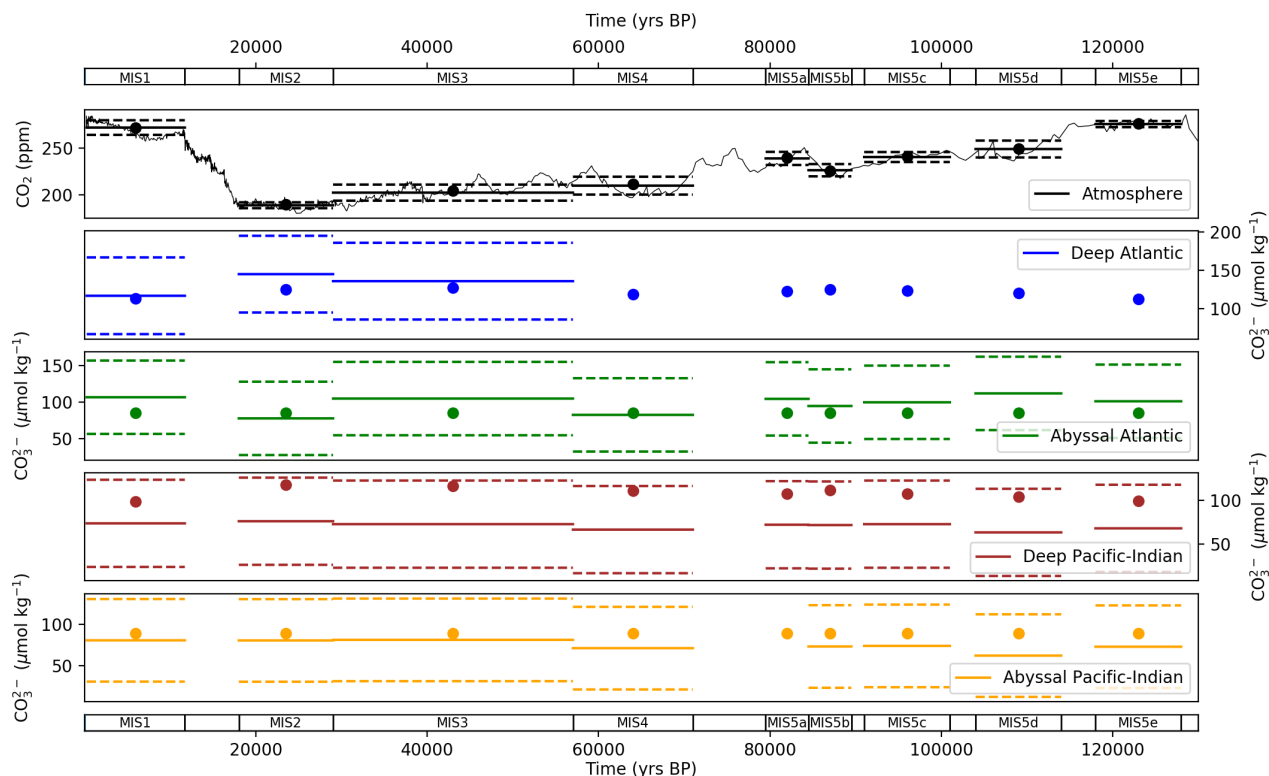


Figure 9. Values returned from the model-data experiment for (A) atmospheric CO_2 and carbonate ion proxy for (B) deep Atlantic, (C) abyssal Atlantic, (D) deep Pacific-Indian and (E) abyssal Pacific-Indian. Model-data experiment results are shown as dots, with mean proxy data shown as solid lines, and one standard deviation range by dashed lines, in each MIS. A default standard deviation of $50 \mu\text{mol kg}^{-1}$ is used as discussed in the text. CO_3^{2-} data for the SCP-M deep Atlantic box in (B) does not extend beyond 50 ka.

The model-data results show good agreement with atmospheric, deep and abyssal $\delta^{13}\text{C}$ data throughout the MIS (Fig. 10). The results mostly fall on the mean and all are within the standard deviation for atmospheric $\delta^{13}\text{C}$ data in the MIS. All results fall within standard deviation for the deep and abyssal Atlantic and Pacific-Indian oceans.

Fig. 11 shows model-data results for atmospheric $\Delta^{14}\text{C}$ and ocean $\Delta\Delta^{14}\text{C}$ compared with data, for MIS 1-3. Model-data results fall within one standard deviation of the data for all observations that were modelled.

Figure 12 shows model-data output for the terrestrial biosphere net primary productivity (NPP) and carbon stock during the glacial cycle. The NPP and carbon stock follow atmospheric CO_2 down in the lead-up to the LGM and rebound from

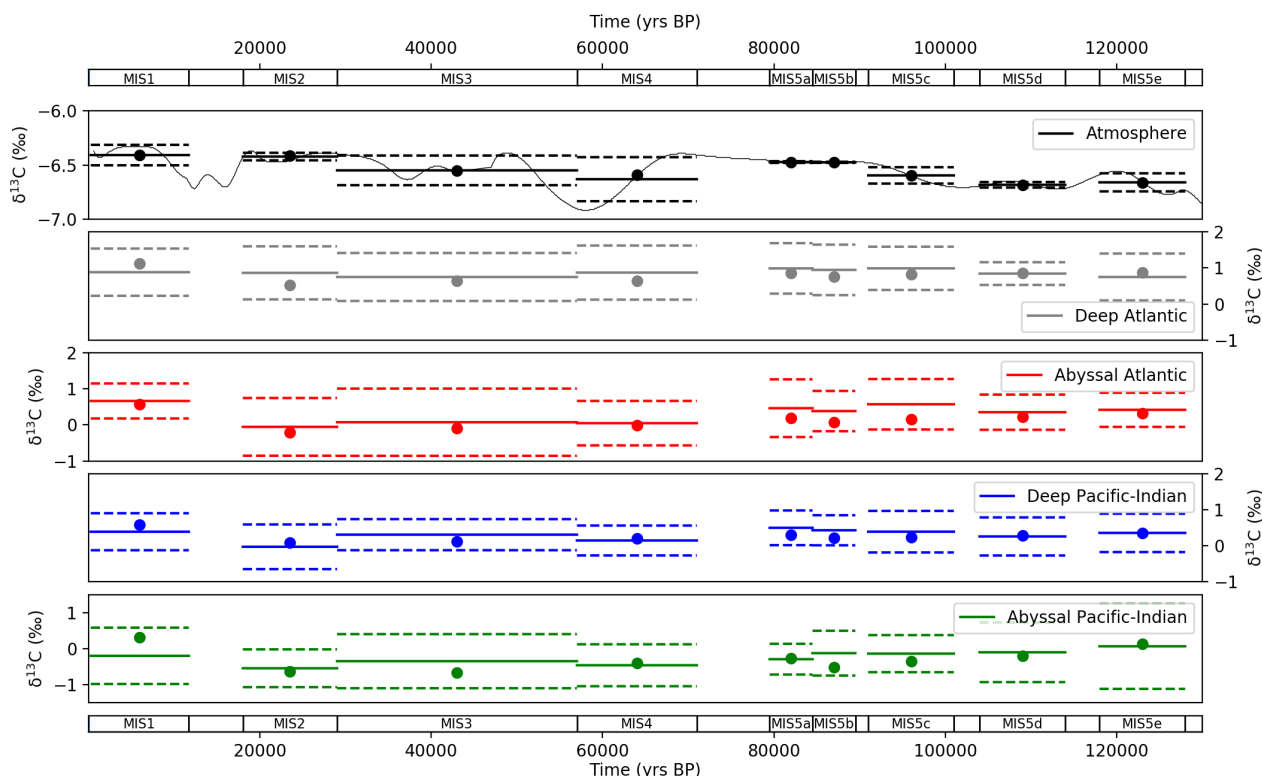


Figure 10. Values returned from the model-data experiment for $\delta^{13}\text{C}$ for (A) atmosphere, (B) deep Atlantic, (C) abyssal Atlantic, (D) deep Pacific-Indian and (E) abyssal Pacific-Indian. Model-data experiment results are shown as dots, with proxy data mean (solid lines) and one standard deviation (dashed lines) in each MIS.

the LGM to the Holocene. This is the effect of carbon fertilisation (Harman et al., 2011; Hoogakker et al., 2016). Notably, there is a distinct drop in NPP at MIS 4, a period where atmospheric CO_2 falls by ~ 30 ppm (Fig. 4(A)). Falling NPP and persistent respiration of the terrestrial biosphere carbon stock during MIS 4, which releases $\delta^{13}\text{C}$ -negative carbon to the atmosphere, can explain the steep drop in atmospheric $\delta^{13}\text{C}$ during the same period (Fig. 4(B)). Hoogakker et al. (2016) provided a reconstruction of NPP through the glacial cycle using pollen data and climate models, shown for comparison in Fig. 12(A). Our model-data results underestimate the Hoogakker et al. (2016) compilation in MIS 5e, but otherwise fall within the range of upper and lower estimates for the other MIS, with slight over-estimation at MIS 5b, 5a, 2 and 1. We model the terrestrial biosphere carbon stock to fall by ~ 500 PgC from the penultimate interglacial to the LGM, and increase by ~ 750 PgC from the LGM to the Holocene (Fig. 12(B)).

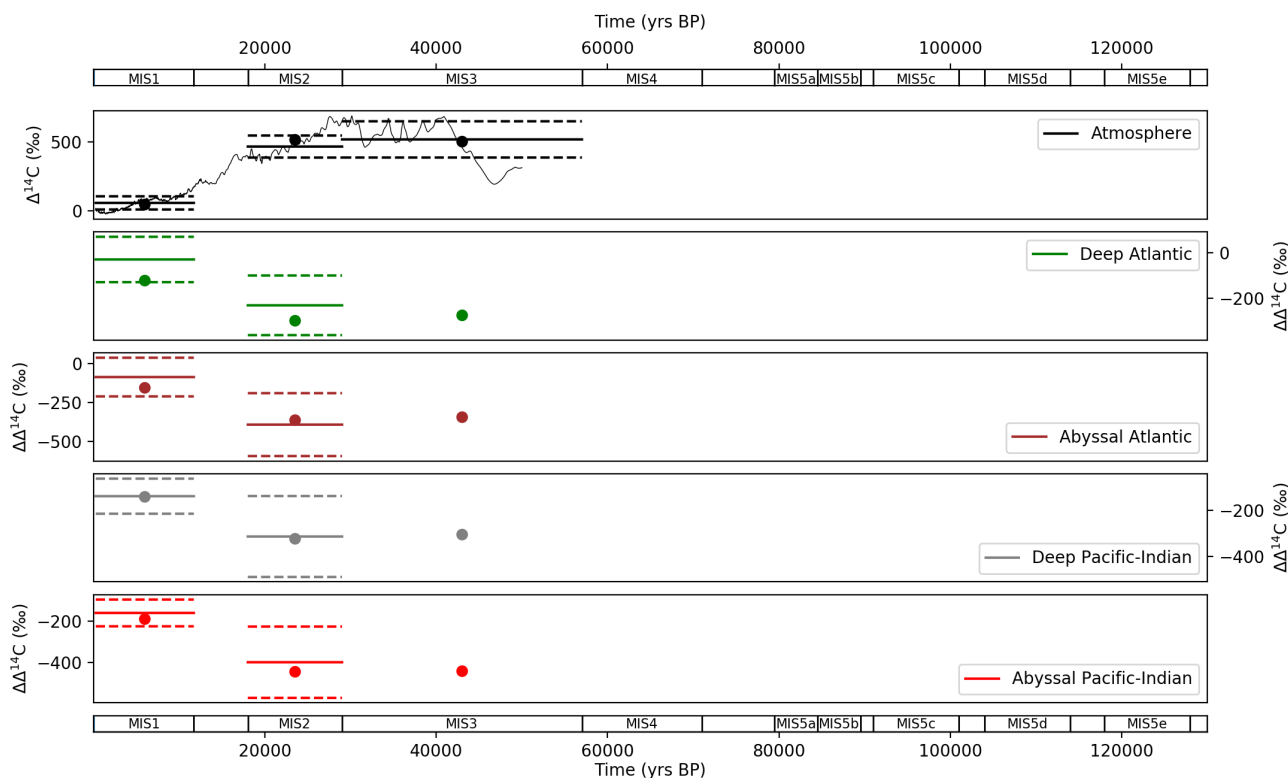


Figure 11. Values returned from the model-data experiment for (A) atmospheric $\Delta^{14}\text{C}$ and $\Delta\Delta^{14}\text{C}$ for (B) deep Atlantic, (C) abyssal Atlantic, (D) deep Pacific-Indian and (E) abyssal Pacific-Indian. $\Delta\Delta^{14}\text{C}$ is atmospheric minus ocean $\Delta^{14}\text{C}$, to correct for the varying atmospheric $\Delta^{14}\text{C}$ signal. Model-data experiment results are shown as dots, with proxy data mean (solid lines) and one standard deviation (dashed lines) in each MIS. Model-data experiment results prior to MIS 4 are omitted, due to the radioactive decay of ^{14}C which precludes natural observations prior to ~ 50 ka.

5 Discussion

5.1 Last glacial cycle

Model simulations constrained by the available data suggest that there were three major episodes in which atmospheric CO_2 fell during the last glacial cycle. The first spanned 120-100 ka (MIS 5d-5e), which resulted in a decrease of ~ 25 ppm. A second drop of ~ 30 ppm occurred during the period 80-60 ka (MIS 4-5a), and finally, a drop of ~ 20 ppm took place more gradually during the period 40-20 ka in the lead up to the LGM (MIS 2-4). The cumulative effect of these discrete events, combined with other minor changes of ~ 10 ppm throughout the glacial lead-up, was a drop in atmospheric CO_2 of ~ 85 ppm

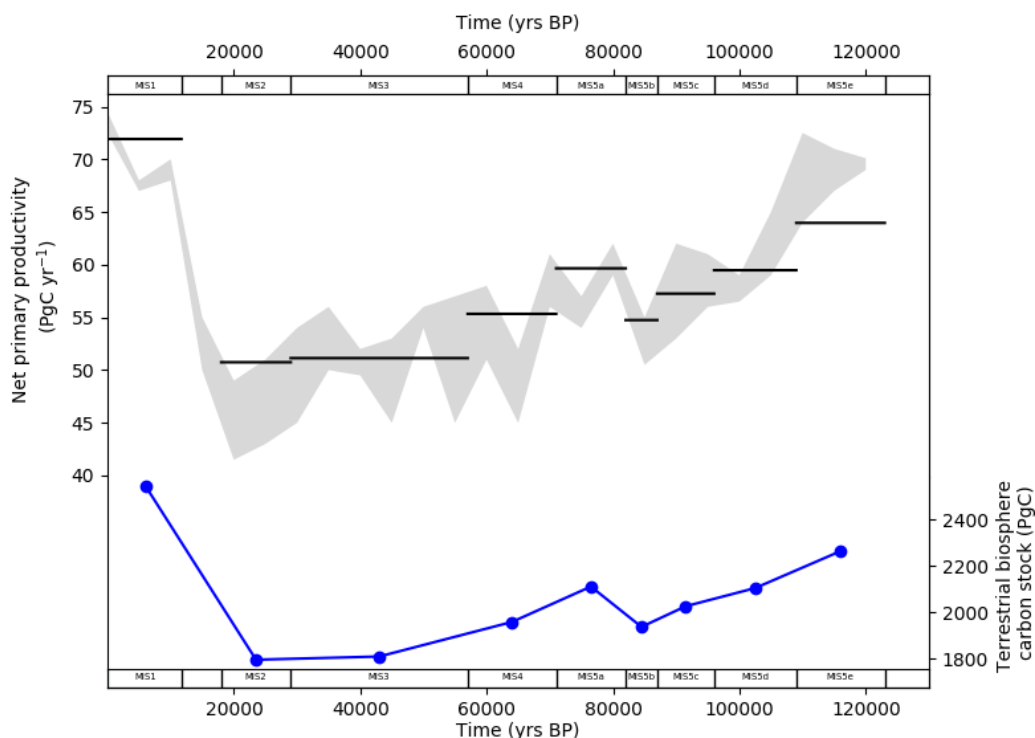


Figure 12. (A) Model-data output for the terrestrial biosphere net primary productivity (NPP) in each MIS time slice (black lines) compared with the range of estimates provided by Hoogakker et al. (2016) (grey area) and (B) model-data output for the terrestrial biosphere carbon stock for each MIS time slice.

below the penultimate interglacial period, ~130-120 ka. Our model-data results show that atmospheric CO₂ and other proxy patterns can be delivered solely by variations in GOC, AMOC and Southern Ocean biological productivity (Figs. 8,9,10,11). Critically, there were also changes in SST, salinity, ocean volume, the terrestrial biosphere, reef carbonates and atmospheric ¹⁴C production (Fig. 2).

- 5 Our model-data results show that the initial fall in CO₂ at MIS 5d was delivered principally by a weakening GOC (Fig. 8). GOC continued to weaken until MIS 5a, then stabilised at MIS 4, before weakening in MIS 3. A pronounced fall in AMOC took place at MIS 4, at the same time that atmospheric CO₂ fell ~30 ppm. GOC and AMOC were both near their lows at the LGM, and accompanied by increased Southern Ocean biological export productivity, yielding the LGM minima in atmospheric CO₂ and the final fall in CO₂ during the glacial cycle. We model elevated Southern Ocean biological productivity during MIS
- 10 2-4, relative to model results for the Holocene (in particular) and for MIS 5a-5d. Importantly, the transition from MIS 3 to MIS 2, which incorporates the LGM and increased Southern Ocean biological productivity, only accounted for an average 13 ppm reduction in CO₂ (Figs. 4,9). Therefore, our results suggest an increase in Southern Ocean biological productivity during



this period was an additional 'kicker' to achieve the LGM CO₂ minima, following prior reductions of ~70 ppm in the lead-up which were delivered mainly by ocean physical processes and SST. The finding of increased biological productivity, while mostly constrained to MIS 2-4, and a modest yet essential contributor to the overall glacial CO₂ drawdown, corroborates proxy data (e.g. Martinez-Garcia et al., 2014; Lambert et al., 2015; Kohfeld and Chase, 2017) and recent model-data exercises (e.g. Menviel et al., 2016; Muglia et al., 2018).

In the Holocene, we model GOC and AMOC returning to values similar to the modern ocean estimates of Talley (2013). Our Holocene result for Atlantic (Pacific-Indian) Southern Ocean biological export productivity, of 2.3 (0.8) mol C m⁻² yr⁻¹ (Fig. 8), falls within modern observations for the Southern Ocean of 0.5-6 mol C m⁻² yr⁻¹ (e.g. Lourey and Trull, 2001; Weeding and Trull, 2004; Ebersbach et al., 2011; Jacquet et al., 2011; Cassar et al., 2015; Arteaga et al., 2019). Our model-data experiment results reproduce values that fall within one standard deviation of the mean value in each model box, for all of the atmosphere and ocean proxies in each MIS (Figs. 9-11).

Kohfeld and Chase (2017) suggested that sequential falls in atmospheric CO₂ were first the result of temperature, sea ice cover and potentially Atlantic Southern Ocean "barrier mechanisms" or shallow stratification, during MIS 5d-5e, and second, followed by falls in deep Atlantic ocean circulation and potentially dust-driven Southern Ocean biological productivity at MIS 4-5a. Finally, a synthesis of those factors with enhanced Southern Ocean biology, delivered the LGM CO₂ minimum. Our model-data results mostly agree with the Kohfeld and Chase (2017) hypothesis for glacial cycle CO₂, however we emphasise the role of ocean circulation in the Pacific and Indian oceans, in addition to the Atlantic Ocean. Stephens and Keeling (2000) proposed that expansive sea-cover around Antarctica, could deliver LGM CO₂ changes on its own as a result of reduced air-sea gas exchange, or in combination with ice-driven ocean stratification. However, Köhler et al. (2010) demonstrated with a carbon cycle box model that increased sea-ice cover leads to increased atmospheric CO₂, due to less in-gassing of CO₂ into the cold waters surrounding Antarctica. Kohfeld and Ridgwell (2009) reviewed estimates of the effects of *decreased* sea ice cover at the last glacial termination and found a best estimate of -5 ppm within a range of -14-0 ppm, which is in the opposite direction to that envisaged by Stephens and Keeling (2000) and Kohfeld and Chase (2017). The modelling work by Stephens and Keeling (2000) was discounted by Kohfeld and Ridgwell (2009), because it assumed nearly all ocean-degassing of CO₂ was confined to the polar Antarctic region, when modern observations suggest the locus of outgassing is in the equatorial ocean (Takahashi et al., 2003). In SCP-M, the effects of polar Southern Ocean sea-ice cover, modelled as a slowing down in air-sea gas exchange in the polar surface box, are modest. This modelling result reflects the offsetting effects of upwelled nutrient- (and carbon) and rich waters (degassing and higher CO₂), against the effects of cooler temperatures and biological export productivity (in-gassing and lower CO₂). Therefore, SCP-M requires other changes in the ocean, to deliver the ~25 ppm fall in CO₂ at MIS 5d-5e. We model a weakening in GOC of ~9 Sv at MIS 5d and minor, further weakening until the LGM, a substantial change outside the Atlantic Basin and underscoring the importance of this feature in any hypothesis for the last glacial cycle or LGM-Holocene (Fig. 8).

The period MIS 5d-5e does not feature in many oceanographic theories of glacial inception, largely due to a focus on Atlantic ocean data and a lack of any obvious changes in the Atlantic shallow-deep-abyssal proxy offsets at that period, as observed at MIS 4 and the LGM (e.g. Oliver et al., 2010; Yu et al., 2016; Kohfeld and Chase, 2017). However, Govin et al. (2009) proposed



an expansion of AABW across the Southern Ocean at MIS 5d, and weakening of circumpolar deep water upwelling, based on qualitative analysis of deep ocean $\delta^{13}\text{C}$ from the Atlantic and Indian basins. This proxy evidence supports the model of De Boer and Hogg (2014) that the glacial ocean could have exhibited slower formation, and at the same time more expansive volume, of AABW. To illustrate the plausibility of a slowdown in GOC in the context of ocean $\delta^{13}\text{C}$ proxy data, we show a model experiment testing the sensitivity of atmospheric CO_2 and abyssal ocean $\delta^{13}\text{C}$ to slowed GOC under MIS 5e conditions (Figure 13). Shown for comparison are the standard deviation of data values for abyssal ocean $\delta^{13}\text{C}$ for MIS 5e. The experiment shows that slowing GOC from the MIS 5e model-data optimised value of 28 Sv (e.g. Fig. 8), delivers lower values for CO_2 and $\delta^{13}\text{C}$. However, despite a range of GOC that almost covers the entire glacial CO_2 drawdown, the abyssal Atlantic $\delta^{13}\text{C}$ result stays within its standard deviation for MIS 5e. Atmospheric CO_2 falls ~ 35 ppm (MIS 5d-5e change is ~ 25 ppm) before one standard deviation is reached for abyssal $\delta^{13}\text{C}$ data, while changes in the deep-abyssal $\delta^{13}\text{C}$ offsets remain muted (Figure 13(C), particularly for the Atlantic Ocean). Therefore, analysing Atlantic Ocean data in isolation, and qualitatively assessing ocean proxy offsets, more generally, may obscure GOC as a feature that could have contributed to glacial falls in atmospheric CO_2 . According to (Talley, 2013) GOC is a key part of the global ocean carbon cycle, operating in the Atlantic, Pacific and Indian ocean basins. A number of authors highlight changes in $\Delta^{14}\text{C}$ distributions in the Pacific Ocean during the LGM and Holocene, providing qualitative evidence of changes in ocean circulation in this basin (e.g. Sikes et al., 2000; Marchitto et al., 2007; Stott et al., 2009; Cook and Keigwin, 2015; Skinner et al., 2015; Ronge et al., 2016; Skinner et al., 2017). However, $\Delta^{14}\text{C}$ proxy records in periods prior to the LGM and Holocene are sparse, because they can only extend to ~ 50 ka due to their radioactive decay in nature.

There is qualitative multi-proxy evidence for a slowdown or shoaling of AMOC at MIS 4. Kohfeld and Chase (2017) evaluated Atlantic basin $\delta^{13}\text{C}$ data and surmised that Atlantic deep ocean circulation slowed or shoaled at MIS 4, and Yu et al. (2016) and Chalk et al. (2019) came to similar conclusions from analysis of carbonate proxy records. Our model-data results corroborate these findings, with a pronounced weakening in AMOC at MIS 4, but we also model a minor, transient drop in AMOC at MIS 5b which replicates abyssal Atlantic $\delta^{13}\text{C}$ and CO_3^{2-} observations (Fig. 5 and Fig. 5), and also accompanies a temporary fall in atmospheric CO_2 of 14 ppm at that period (Fig. 4). SCP-M does not take account of AMOC shoaling due to its rigid box boundaries, and therefore the change in proxy data across MIS 4-5a is resolved as weakening AMOC, which could understate the importance of this event.

Figure 14 shows the contribution to the glacial drawdown in atmospheric CO_2 by each mechanism we modelled, relative to the penultimate interglacial period (MIS 5e), in SCP-M. Weakened GOC delivers the highest contribution to falling CO_2 , followed by cooler SST, weakened AMOC and stronger Southern Ocean biological export productivity. Lower SST leads to modest reductions in CO_2 early in the glacial cycle, increasing as the ocean cools further in MIS 4, and is an important contributor to decreased CO_2 in the LGM (Kohfeld and Chase, 2017). Southern Ocean biological export productivity weakens initially, from MIS 5e to 5d, then strengthens relative to MIS 5a-5d, at MIS 4, and contributes ~ 12 ppm during MIS 2 (LGM). Other parameters contribute minor increases in CO_2 (salinity, polar sea ice, ocean volume) and decreases (coral reefs) during the cycle. Our estimate for coral reefs, of -7 ppm CO_2 , is at the lower range of 6-20 ppm summarised in Kohfeld and Ridgwell (2009), suggesting that our simple parameterisation of the coral reef carbon and alkalinity fluxes could underestimate its effect,

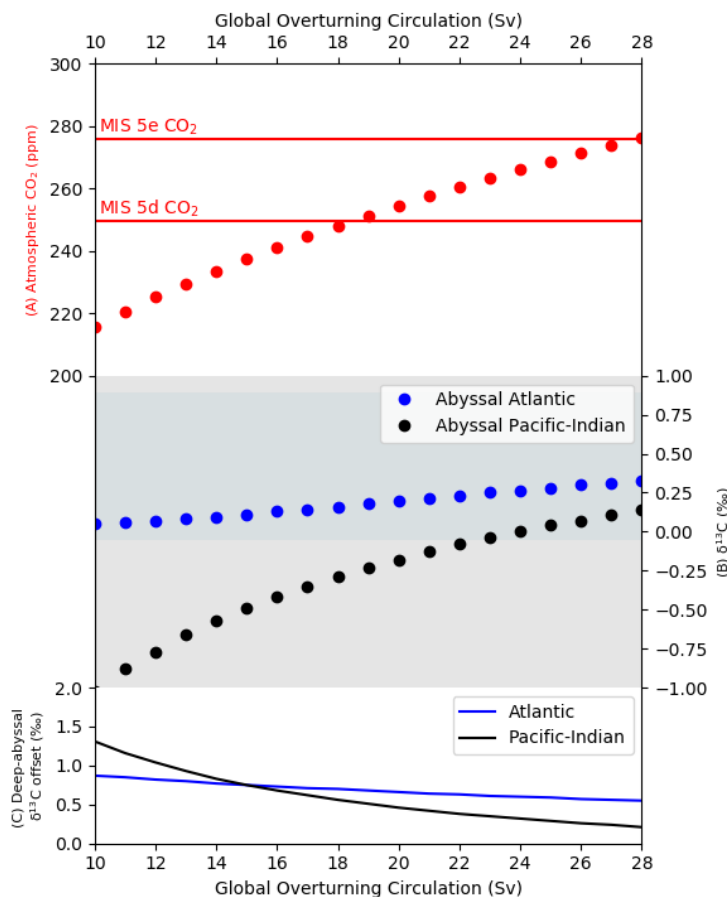


Figure 13. Sensitivity of atmospheric CO₂ and ocean δ¹³C to a downward variation in global ocean circulation parameter Ψ_1 in MIS 5e in SCP-M. x-axis shows the range of variation in Ψ_1 in Sv and the y-axes show the model results for (A) atmospheric CO₂ and (B) abyssal ocean δ¹³C in each basin. Shaded areas are the ± standard deviations for abyssal δ¹³C in MIS 5e. (C) shows the deep-abyssal δ¹³C offset for each basin. Atmospheric CO₂ in MIS 5d and 5e is shown for reference. All other model settings per MIS 5e.

likely due to the assumed fast mixing rates of reef carbon and alkalinity into the surface boxes in SCP-M. Ridgwell et al. (2003) modelled +20 ppm CO₂ from coral reef accumulation in the Holocene period, noting a high sensitivity of their model to coral reef accumulation rates.

5.2 The LGM and Holocene

- 5 Within the context of LGM-Holocene studies, our findings corroborate the hypothesis that a number of mechanisms, not one singular factor, delivered the ~85 ppm increase in atmospheric CO₂ from the LGM to the Holocene (e.g. Kohfeld and Ridgwell, 2009; Sigman et al., 2010; Hain et al., 2010; Ferrari et al., 2014; Menviel et al., 2016; Kohfeld and Chase, 2017;

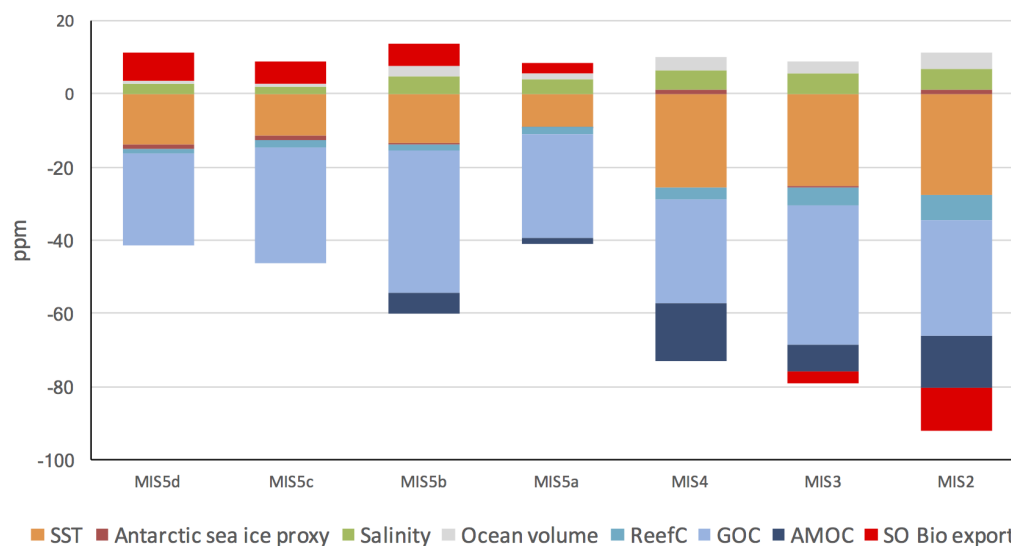


Figure 14. Impacts on CO₂ of model parameters from the model-data experiment results, from the penultimate interglacial period (MIS 5e) to the Last Glacial Maximum (MIS 2). SST = sea surface temperature, ReefC = shallow carbonate production/dissolution, GOC = global ocean circulation, AMOC = Atlantic Meridional Overturning Circulation, SO Bio Export = Southern Ocean Biological export productivity.

Muglia et al., 2018). This finding is more obvious when the sequential nature of changes is observed over the full glacial cycle, as distinct from analysing the LGM and Holocene in isolation. Our model-data results agree with those of Menviel et al. (2016): that variations primarily in GOC and AMOC, and alongside Southern Ocean biological productivity, can account for for atmospheric CO₂ variation from the LGM to the Holocene, with an opposing feedback provided by the terrestrial biosphere.

- 5 The longer time timescale of our analysis highlights that changes in GOC and AMOC took place much earlier in the glacial cycle than the LGM, and were at or near their glacial minima prior to the LGM. Our model-data results also constrain the effects of Southern Ocean biological export productivity in the glacial cycle CO₂, to MIS 2-4. Enhanced wind-borne iron dust deposits over the Southern Ocean are believed to have fed increased phytoplankton growth in the LGM and possibly MIS 4 (Martin, 1990; Martinez-Garcia et al., 2014; Kohfeld and Chase, 2017; Muglia et al., 2018).

10 5.3 The terrestrial biosphere

Our modelled variation in the terrestrial biosphere from the LGM to Holocene, of ~750 Pg C (Fig. 12), is at the upper bound of recent estimates of this change, of 0-700 Pg C (e.g. Ciais et al., 2012), Peterson et al. (2014)), but within uncertainty bounds. For example, Peterson et al. (2014) estimated a variation of 511 ± 289 Pg C in the terrestrial biosphere carbon stock, based on whole of ocean $\delta^{13}\text{C}$ data. According to Francois et al. (1999), palynological and sediment data infer that the terrestrial biosphere carbon stock was 700-1350 PgC smaller in the LGM than the present. Ciais et al. (2012) pointed to a growth of a



large inert carbon pool in steppes and tundra during the LGM as an offsetting feature to the declining tropical biosphere, a feature included in reconstructed last glacial terrestrial biosphere by Hoogakker et al. (2016). While our model results are at the upper end of recent modelled and qualitative estimates of the LGM-Holocene change in the terrestrial biosphere, they are in agreement with the glacial cycle reconstruction of NPP of Hoogakker et al. (2016) as shown in Fig. 12.

5 5.4 Advantages and limitations of this study

The use of a simple box model for this model-data study, SCP-M, enabled a range of proxies to be incorporated into the MIS reconstructions, and a large number of simulations (~5,000) to explore possible parameter combinations in each MIS. However, given the large spatial coverage of the SCP-M boxes, data for large areas of the ocean are averaged, and some detail is lost. For example, in the case of the carbonate ion proxy, we apply a default estimate of standard deviation to account for the large volume of ocean covered by SCP-M's boxes relative to the proxy data locations, and to enable the normalisation of the carbonate ion proxy data in a procedure that uses the data standard deviation as a weighting. Despite this caveat, we believe that the model-data experiment results provide a good match to the data across the various atmospheric and ocean proxies as shown in Figs 9-11.

Most major processes in the model are simply parameterised, allowing them to be free-floated in model-data experiments. The driving factors behind parameter value changes can only be speculated. For example, slowdown in GOC may be the result of changing wind patterns or buoyancy fluxes around Antarctica (Morrison and Hogg, 2013), Antarctic sea-ice cover (Ferrari et al., 2014), or may be the result of shoaling AMOC leading to extensive filling of the abyssal ocean by waters sourced from GOC (Curry and Oppo, 2005; De Boer and Hogg, 2014; Jansen, 2017). Probing the root cause of our model-data findings would require a more detailed physical and/or biogeochemical model. Our MIS time-slicing may obscure detail in the proxy records within MIS. For example, Yu et al. (2013) observed a transient drop in carbonate ion concentrations in the deep Pacific Ocean during MIS 4. We omit the transient last glacial termination, a period in which atmospheric CO₂ rose ~85 ppm in 8 kyr. Future work could probe this period at 1 kyr intervals, or with transient simulations, to profile the unwinding of processes that led to the last glacial cycle CO₂ drawdown.

6 Conclusions

Multiple processes drove atmospheric CO₂ fluctuations during the last glacial cycle. Against a backdrop of varied SST, salinity, sea-ice cover, ocean volume and reef carbonates, we modelled sequentially weaker GOC (first) and AMOC (second) to reduce atmospheric CO₂ in the lead up to the LGM. At the LGM, increased Southern Ocean biological export productivity delivered an incremental fall in CO₂, resulting in the glacial cycle CO₂ minimum. GOC, AMOC, Southern Ocean biology and SST rebounded to modern values between the LGM and Holocene, contributing to the sharp post-glacial increase in CO₂. The terrestrial biosphere played an important negative feedback role during the glacial cycle, releasing δ¹³C-negative CO₂ to the atmosphere at times during the glaciation, and taking up CO₂ during the termination and Holocene. These model-data results were achieved with a simple carbon cycle box optimised for proxy data for CO₂, δ¹³C, Δ¹⁴C and CO₂²⁻³. Our results agree



with composite hypotheses for glacial cycle CO₂ that emphasise varying ocean circulation (e.g. Kohfeld and Ridgwell, 2009; Sigman et al., 2010; Ferrari et al., 2014; Menviel et al., 2016; Kohfeld and Chase, 2017), include marine biological productivity, and amidst many other changes in the marine and terrestrial carbon cycle. We emphasise the need to include the Pacific and Indian oceans in evaluation of the oceanic carbon cycle, particularly in relation to the last glacial cycle and the LGM-Holocene transition.

Many uncertainties exist in the data and the prescribed nature of the processes in a box model. However, such uncertainty is largely inescapable when dealing with models and proxy data. We propose these model-data results as one set of plausible results for the last glacial carbon cycle, in agreement with available proxy data, and see them as encouraging for the use of models and data to help constrain hypotheses for the paleo- carbon cycle.

7 Code and data availability

The model code, processed data files, model-data experiment results, and any (published) raw proxy data gathered in the course of this work, are located at <https://doi.org/10.5281/zenodo.3559339>. No original data was created, or unpublished data used, in this work. This paper's Supplementary Information contains an overview of the files contained in the repository. For more detail on the SCP-M equations, see O'Neill et al. (2019).

Author contributions. CO undertook model development work, data-gathering, modelling and model-data experiments. AH provided the oceanographic interpretation and guided modelling and data analysis. ME designed model-data experiments and provided input into data analysis and the modelling of the marine biology and isotopes. BO contributed glacial cycle model forcings and input to modelling of the reef carbonates. SE oversaw the modelling of the marine biology and carbonate pump. All authors contributed to drafting and reviewing the document.

Competing interests. The authors declare that they have no conflict of interest.

Acknowledgements. Stewart Fallon provided input to the processing of radiocarbon data. Malcolm Sambridge provided input on model-data optimisation and inversions. Jimin Yu provided helpful discussions and carbonate ion proxy data.



References

- Adkins, J., McIntyre, K., and Schrag, D.: The Salinity, Temperature, and 18O of the Glacial Deep Ocean, *Science*, 298, 1769–1773, 2002.
- Anderson, R., Chase, Z., Fleisher, M., and Sachs, J.: The Southern Ocean’s biological pump during the Last Glacial Maximum, *Deep Sea Research Part II: Topical Studies in Oceanography*, 49, 1909–1938, 2002.
- 5 Artega, L., Pahlow, M., Bushinsky, S., and Sarmiento, J.: Nutrient Controls on Export Production in the Southern Ocean, *Global Biogeochemical Cycles*, 33, 942–956, 2019.
- Barker, S., Knorr, G., Vautravers, M., Diz, P., and Skinner, L.: Extreme deepening of the Atlantic overturning circulation during deglaciation, *Nature Geoscience*, 3, 567–571, 2010.
- Bereiter, B., Eggleston, S., Schmitt, J., Nehrbass-Ahles, C., Stocker, T., Fischer, H., Kipfstuhl, S., and Chappellaz, J.: Revision of the EPICA
10 Dome C CO_2 record from 800 to 600kyr before present, *Geophys. Res. Lett.*, 2015.
- Broecker, W., Yu, J., and Putnam, A.: Two contributors to the glacial CO_2 decline, *Earth and Planetary Science Letters*, pp. 191–196, 2015.
- Broecker, W. S.: Ocean chemistry during glacial time, *Geochim. Cosmochim. Acta*, 46, 1689–1705, 1982.
- Broecker, W. S. and Barker, S.: A 190‰ drop in atmosphere’s $\Delta^{14}\text{C}$ during the “Mystery Interval” (17.5 to 14.5 kyr), *Earth and Planetary Science Letters*, 256, 90–99, 2007.
- 15 Bryan, S., Marchitto, T., and Lehman, S.: The release of ^{14}C -depleted carbon from the deep ocean during the last deglaciation: Evidence from the Arabian Sea, *Earth and Planetary Science Letters*, 298, 244–254, 2010.
- Burke, A. and Robinson, L.: The Southern Ocean’s Role in Carbon Exchange During the Last Deglaciation, *Science*, 335, 557–561, 2012.
- Cassar, N., Wright, S., Thomson, P., Trull, T., Westwood, K., de Salas, M., Davidson, A., Pearce, I., Davies, D., and Matear, R.: The relation of mixed-layer carbon export production to plankton community in the Southern Ocean, *Global Biogeochemical Cycles*, 29, 446–462,
20 2015.
- Chalk, T., Foster, G., and Wilson, P.: Dynamic storage of glacial CO_2 in the Atlantic Ocean revealed by boron [$\text{CO}_2\text{-3}$] and pH records, *Earth and Planetary Science Letters*, 510, 1–11, 2019.
- Chen, T., Robinson, L., Burke, A., Southon, J., Spooner, P., Morris, P., and Ng, H.: Synchronous centennial abrupt events in the ocean and atmosphere during the last deglaciation, *Science*, 349, 1537–1541, 2015.
- 25 Ciais, P., Tagliabue, A., Cuntz, M., Bopp, L., Scholze, M., Hoffmann, G., Laurantou, A., Harrison, S. P., Prentice, I. C., Kelley, D. I., Koven, C., and Piao, S. L.: Large inert carbon pool in the terrestrial biosphere during the Last Glacial Maximum, *Nature Geoscience*, 5, 74–79, 2012.
- Cook, M. and Keigwin, L.: Radiocarbon profiles of the NW Pacific from the LGM and deglaciation: Evaluating ventilation metrics and the effect of uncertain surface reservoir ages, *Paleoceanography*, pp. 174–195, 2015.
- 30 Curry, W. B. and Oppo, D. W.: Glacial water mass geometry and the distribution of $\delta^{13}\text{C}$ of CO_2 in the western Atlantic Ocean, *Paleoceanography*, 20, PA1017, doi:10.1029/2004PA001021, 2005.
- Davies-Walczak, M., Mix, A., Stoner, J., Southon, J., Cheseby, M., and Xuan, C.: Late Glacial to Holocene radiocarbon constraints on North Pacific Intermediate Water ventilation and deglacial atmospheric CO_2 sources, *Earth and Planetary Science Letters*, 397, 57–66, 2014.
- De Boer, A. M. and Hogg, A. M. C.: Control of the glacial carbon budget by topographically induced mixing, *Geophys. Res. Lett.*, 41,
35 4277–4284, 2014.
- DeVries, T. and Weber, T.: The export and fate of organic matter in the ocean: New constraints from combining satellite and oceanographic tracer observations, *Paleoceanography*, 31, 535–555, 2017.



- Dunne, J. P., Armstrong, R. A., Gnanadesikan, A., and Sarmiento, J. L.: Empirical and mechanistic models for the particle export ratio, *Global Biogeochemical Cycles*, 19, GB4026, doi:10.1029/2004GB002390, 2005.
- Ebersbach, F., Trull, W., Davies, D., and Bray, S.: Controls on mesopelagic particle fluxes in the Sub-Antarctic and Polar Frontal Zones in the Southern Ocean south of Australia in summer - Perspectives from free-drifting sediment traps, *Deep Sea Research Part II: Topical Studies in Oceanography*, 58, 2260–2276, 2011.
- Egglegston, S., Schmitt, J., Bereiter, B., Schneider, R., and Fischer, H.: Evolution of the stable carbon isotope composition of atmospheric CO₂ over the last glacial cycle, *Paleoceanography*, 31, 434–452, 2016.
- Ferrari, R., Jansen, M., Adkins, J., Burke, A., Stewart, A. L., and Thompson, A.: Antarctic sea ice control on ocean circulation in present and glacial climates, *PNAS*, 111, 8753–8758, 2014.
- 10 Francois, L., Godderis, Y., Warnant, P., Ramstein, G., de Noblet, N., and Lorenz, S.: Carbon stocks and isotopic budgets of the terrestrial biosphere at mid-Holocene and last glacial maximum times, *Chemical Geology*, 159, 163–199, 1999.
- Freeman, E., Skinner, L., Waelbroeck, C., and Hodell, D.: Radiocarbon evidence for enhanced respired carbon storage in the Atlantic at the Last Glacial Maximum, *Nature Communications*, 2016.
- Govin, A., Michel, E., Labeyrie, L., Waelbroeck, C., Dewilde, F., and Jansen, E.: Evidence for northward expansion of Antarctic Bottom Water mass in the Southern Ocean during the last glacial inception, *Paleoceanography*, 24, doi:10.1029/2008PA001603, 2009.
- 15 Hain, M. P., Sigman, D. M., and Haug, G. H.: Carbon dioxide effects of Antarctic stratification, North Atlantic Intermediate Water formation, and subantarctic nutrient drawdown during the last ice age: Diagnosis and synthesis in a geochemical box model, *Global Biogeochemical Cycles*, 24, GB4023, doi:10.1029/2010GB003790, 2010.
- Harman, I., Trudinger, C., and Raupach, M.: SCCM – the Simple Carbon-Climate Model: Technical Documentation, CAWCR Technical Report 047, CSIRO Centre for Australian Weather and Climate Research, CSIRO Marine and Atmospheric Research, FC Pye Laboratory, GPO Box 3023, Canberra, ACT, 2601, Australia, 2011.
- 20 Henson, S. A., Sanders, R., Madsen, E., Morris, P. J., Moigne, F. L., and Quartly, G. D.: A reduced estimate of the strength of the ocean’s biological carbon pump, *Geophys. Res. Lett.*, 38, L04606, doi:10.1029/2011GL046735, 2011.
- Hines, S., Southon, J., and Adkins, J.: A high-resolution record of Southern Ocean intermediate water radiocarbon over the past 30,000 years, *Earth and Planetary Science Letters*, 432, 46–48, 2015.
- 25 Hoff, U., Rasmussen, T., Stein, R., Ezat, M., and Fahl, K.: Sea ice and millennial-scale climate variability in the Nordic seas 90 kyr ago to present, *Nature Communications*, 7, DOI: 10.1038/ncomms12247, 2015.
- Hogg, A. M.: Glacial cycles and carbon dioxide: A conceptual model, *Geophys. Res. Lett.*, 35, L01701, doi:10.1029/2007GL032071, 2008.
- Hoogakker, B. et al.: Terrestrial biosphere changes over the last 120 kyr, *Climate of the Past*, 12, 51–73, 2016.
- 30 Jacquet, S., Lam, P., Trull, T., and Dehairs, F.: Carbon export production in the Polar Front Zone and Subantarctic Zone south of Tasmania, *Deep Sea Research Part II: Topical Studies in Oceanography*, 58, 2277–2292, 2011.
- Jansen, M.: Glacial ocean circulation and stratification explained by reduced atmospheric temperature, *PNAS*, 114, 45–50, 2017.
- Key, R.: Ocean process tracers: Radiocarbon. In: *Encyclopedia of Ocean Sciences*, pp. 2338–2353, Academic Press, London, 2001.
- Key, R., Kozyr, A., Sabine, C. L., Lee, K., Wanninkhof, R., Bullister, J. L., Feely, R. A., Millero, F. J., Mordy, C., and Peng, T.-H.: A global ocean carbon climatology: Results from Global Data Analysis Project (GLODAP), *Global Biogeochemical Cycles*, 18, GB4031, doi:10.1029/2004GB002247, 2004.
- 35 Kleypas, J.: Modeled estimates of global reef habitat and carbonate production since the Last Glacial Maximum, *Paleoceanography and Paleoclimatology*, 12, 533–545, 1997.



- Knox, F. and McElroy, M.: Changes in Atmospheric CO₂: Influence of the Marine Biota at High Latitude, *Journal of Geophysical Research*, 89, 4269–4637, 1984.
- Kohfeld, K. and Chase, Z.: Temporal evolution of mechanisms controlling ocean carbon uptake during the last glacial cycle, *Earth and Planetary Science Letters*, 472, 206–215, 2017.
- 5 Kohfeld, K. and Ridgwell, A.: Glacial-Interglacial Variability in Atmospheric CO₂, *Surface Ocean–Lower Atmosphere Processes*, *Geophysical Research Series*, 187, 251–286, 2009.
- Kohfeld, K., Quéré, C. L., Harrison, S., and Anderson, R.: Role of Marine Biology in Glacial-Interglacial CO₂ Cycles, *Science*, 308, 74–78, 2005.
- Köhler, P., Fischer, H., and Schmitt, J.: Atmospheric δ¹³C_{CO2} and its relation to pCO₂ and deep ocean δ¹³C during the late Pleistocene, 10 *Paleoceanography*, 25, doi:10.1029/2008PA001703, 2010.
- Kurahashi-Nakamura, T., Paul, A., and Losch, M.: Dynamical reconstruction of the global ocean state during the Last Glacial Maximum, *Paleoceanography*, 32, 326–350, 2017.
- Lambert, F., Tagliabue, A., Shaffer, G., Lamy, F., Winckler, G., Farias, L., Gallardo, L., and Pol-Holz, D.: Dust fluxes and iron fertilization in Holocene and Last Glacial Maximum climates, *Geophysical Research Letters*, 42, 6014–6023, 2015.
- 15 Lisiecki, L. E. and Raymo, M. E.: A Pliocene-Pleistocene stack of 57 globally distributed benthic δ¹⁸O records, *Paleoceanography*, 20, doi:10.1029/2004PA001071, 2005.
- Liu, C., Kohl, A., Liu, Z., Wang, F., and Stammer, D.: Deep-reaching thermocline mixing in the equatorial Pacific cold tongue, *Nature Communications*, 7, 11576, doi:10.1038/ncomms11576, 2016.
- Lourey, M. J. and Trull, W.: Seasonal nutrient depletion and carbon export in the Subantarctic and Polar Frontal Zones of the Southern Ocean 20 south of Australia, *Journal of Geophysical Research: Oceans*, 106, 31463–31487, 2001.
- Maffezzoli, N., Vallelonga, P., Edwards, R., Saiz-Lopez, A., Turetta, C., Kjær, H. A., Barbante, C., Vinther, B., and Spolaor, A.: 120,000 year record of sea ice in the North Atlantic, *Climate of the Past*, 2018, 1–19, 2018.
- Marchitto, T., Lehman, S., Ortiz, J., Flückiger, J., and van Geen, A.: Marine Radiocarbon Evidence for the Mechanism of Deglacial Atmospheric CO₂ Rise, *Science*, 316, 1456–1459, 2007.
- 25 Martin, J.: Glacial-interglacial CO₂ change: The Iron Hypothesis, *Paleoceanography*, 5, 1–13, 1990.
- Martin, J. H., Knauer, G., Karl, D., and Broenkow, W.: VERTEX: carbon cycling in the northeast Pacific, *Deep-Sea Research*, 34, 267–285, 1987.
- Martinez-Garcia, A., Sigman, D., H. Ren, Anderson, R., Straub, M., Hodell, D., Jaccard, S., Eglinton, T., and Haug, G.: Iron Fertilization of the Subantarctic Ocean During the Last Ice Age, *Science*, 343, 1347–1350, 2014.
- 30 Menviel, L., Yu, J., Joos, F., Mouchet, A., Meissner, K. J., and England, M. H.: Poorly ventilated deep ocean at the Last Glacial Maximum inferred from carbon isotopes: A data-model comparison study, *Paleoceanography*, 31, 2–17, 2016.
- Morrison, A. and Hogg, A.: On the Relationship between Southern Ocean Overturning and ACC Transport, *Journal of Physical Oceanography*, 43, 140–148, 2013.
- Muglia, J., Skinner, L., and Schmittner, A.: Weak overturning circulation and high Southern Ocean nutrient utilization maximized glacial 35 ocean carbon, *Earth and Planetary Science Letters*, 496, 47–56, 2018.
- Muscheler, R., Beer, J., Wagner, G., Laj, C., Kissel, C., Raisbeck, G., Yioud, F., and Kubik, P.: Changes in the carbon cycle during the last deglaciation as indicated by the comparison of ¹⁰Be and ¹⁴C records, *Earth and Planetary Science Letters*, 219, 325–340, 2014.



- Oliver, K., Hoogakker, B., Crowhurst, S., Henderson, G., Rickaby, R., Edwards, N., and Elderfield, H.: A synthesis of marine sediment core $\delta^{13}\text{C}$ data over the last 150 000 years, *Climate of the Past*, 6, 645–673, 2010.
- O'Neill, C., A. Mc. Hogg, M.J. Ellwood, S. E., and Opdyke, B.: The [simple carbon project] model v1.0, *Geosci. Model Dev.*, 12, 1541–1572, <https://doi.org/10.5194/gmd-12-1541-2019>, 2019.
- 5 Opdyke, B. and Walker, J.: Return of the coral reef hypothesis: Basin to shelf partitioning of CaCO_3 and its effect on atmospheric CO_2 , *Geology*, 20, 733–736, 1992.
- Peterson, C. D., Lisiecki, L. E., and Stern, J. V.: Deglacial whole-ocean $\delta^{13}\text{C}$ change estimated from 480 benthic foraminiferal records, *Paleoceanography*, 29, 549–563, 2014.
- Qin, B., Li, T., Xiong, Z., Algeo, T. J., and Chang, F.: Deepwater carbonate ion concentrations in the western tropical Pacific since 250 ka:
10 Evidence for oceanic carbon storage and global climate influence, *Paleoceanography*, 32, 351–370, 2017.
- Qin, B., Li, T., Xiong, Z., Algeo, T., and Jia, Q.: Deep-Water Carbonate Ion Concentrations in the Western Tropical Pacific Since the Mid-Pleistocene: A Major Perturbation During the Mid-Brunhes, *Journal of Geophysical Research: Oceans*, 123, <https://doi.org/10.1029/2018JC014084>, 2018.
- Reimer, P., Baillie, M., Bard, E., Bayliss, A., Beck, J., Blackwell, P., Ramsey, C. B., Buck, C., Burr, G., Edwards, R., Friedrich, M., Grootes, P., Guilderson, T., Hajdas, I., Heaton, T., Hogg, A., Hughen, K., Kaiser, K., Kromer, B., McCormac, F., Manning, S., Reimer, R., Richards, D., Southon, J., Talamo, S., Turney, C., van der Plicht, J., and Weyhenmeyer, C.: IntCal09 and Marine09 radiocarbon age calibration curves, 0–50,000 years cal BP., *Radiocarbon*, 51, 1111–50, 2009.
- Ridgwell, A., Watson, A., Maslin, M., and Kaplan, J.: Implications of coral reef buildup for the controls on atmospheric CO_2 since the Last Glacial Maximum, *Paleoceanography*, 18, 1083, doi:10.1029/2003PA000893, 2003.
- 20 Rohling, E., Grant, K., Bolshaw, M., Roberts, A., Siddall, M., Hemleben, C., and Kucera, M.: Antarctic temperature and global sea level closely coupled over the past five glacial cycles, *Nature Geoscience*, 2, 500–504, 2009.
- Ronge, T., Tiedemann, R., Lamy, F., Kohler, P., Alloway, B., Pol-Holz, R. D., Pahnke, K., Southon, J., and Wacker, L.: Radiocarbon constraints on the extent and evolution of the South Pacific glacial carbon pool, *Nature Communications*, 7, 11487, doi:10.1038/ncomms11487, 2016.
- 25 Sarmiento, J. L. and Gruber, N.: *Ocean biogeochemical dynamics*, Princeton University Press, 2006.
- Sarmiento, J. L. and Toggweiler, J. R.: A new model for the role of the oceans in determining atmospheric CO_2 , *Nature*, 308, 621–624, 1984.
- Schmitt, J., Schneider, R., Elsig, J., Leuenberger, D., Lourdou, A., Chappellaz, J., Köhler, P., Joos, F., Stocker, T., Leuenberger, M., and Fischer, H.: Carbon Isotope Constraints on the Deglacial CO_2 Rise from Ice Cores, *Science*, 336, 711–714, 2012.
- Siegel, D. A., Buesseler, K. O., Doney, S. C., Saille, S. F., Behrenfeld, M. J., and Boyd, P. W.: Global assessment of ocean carbon export by
30 combining satellite observations and foodweb models, *Global Biogeochemical Cycles*, 28, 181–196, 2014.
- Sigman, D. and Boyle, E.: Glacial/interglacial variations in atmospheric carbon dioxide, *Nature Reviews*, 407, 859–869, 2000.
- Sigman, D., Hain, M., and Haug, G.: The polar ocean and glacial cycles in atmospheric CO_2 concentration, *Nature Reviews*, 466, 47–55, 2010.
- Sikes, E., Samson, C., Guilderson, T., and Howard, W.: Old radiocarbon ages in the southwest Pacific Ocean during the last glacial period and deglaciation, *Nature*, 405, 555–559, 2000.
- 35 Sikes, E., Cook, M., and Guilderson, T.: Reduced deep ocean ventilation in the Southern Pacific Ocean during the last glaciation persisted into the deglaciation, *Earth and Planetary Science Letters*, 438, 130–138, 2016.



- Skinner, L. and Shackleton, N. J.: Rapid transient changes in northeast Atlantic deep water ventilation age across Termination I, *Paleoceanography*, 19, PA2005, doi:10.1029/2003PA000983, 2004.
- Skinner, L., Waelbroeck, C., Scrivner, A., and Fallon, S.: Radiocarbon evidence for alternating northern and southern sources of ventilation of the deep Atlantic carbon pool during the last deglaciation, *PNAS*, 111, 2014.
- 5 Skinner, L., McCave, I., Carter, L., Fallon, S., Scrivner, A., and Primeau, F.: Reduced ventilation and enhanced magnitude of the deep Pacific carbon pool during the last glacial period, *Earth and Planetary Science Letters*, 411, 45–52, 2015.
- Skinner, L., Primeau, F., Freeman, E., de la Fuente, M., Goodwin, P. A., Gottschalk, J., Huang, E., McCave, I. N., Noble, T. L., and Scrivner, A. E.: Radiocarbon constraints on the glacial ocean circulation and its impact on atmospheric CO₂, *Nature Communications*, 8, 16010, doi: 10.1038/ncomms16010, 2017.
- 10 Skinner, L. C., Fallon, S., Waelbroeck, C., Michel, E., and Barker, S.: Ventilation of the Deep Southern Ocean and Deglacial CO₂ Rise, *Science*, 328, 1147–1151, 2010.
- Stephens, B. and Keeling, R.: The influence of Antarctic sea ice on glacial-interglacial CO₂ variations, *Nature*, 404, 171–174, 2000.
- Stott, L., Southon, J., Timmermann, A., and Koutavas, A.: Radiocarbon age anomaly at intermediate water depth in the Pacific Ocean during the last deglaciation, *Paleoceanography*, 24, 2009.
- 15 Strutz, T.: *Data Fitting and Uncertainty. A practical introduction to weighted least squares and beyond.*, vol. 2 of *Wiesbaden*, Springer Vieweg, 2016.
- Takahashi, T., Sutherland, S., Feely, R., and Cosca, C.: Decadal variation of the surface water PCO₂ in the western and central equatorial Pacific, *Science*, 302, 852–856, 2003.
- Talley, L.: Closure of the global overturning circulation through the Indian, Pacific, and Southern Oceans: Schematics and transports, *Oceanography*, 78, 257–303, 2013.
- 20 Toggweiler, J. and Sarmiento, J.: Glacial to interglacial changes in atmospheric carbon dioxide: The critical role of ocean surface water in high latitudes, in *The Carbon Cycle and Atmospheric CO₂: Natural Variations Archean to Present*, Geophysical Monograph Series, American Geophysical Union, 32, 163–184, 1985.
- Toggweiler, J. R.: Variation of atmospheric CO₂ by ventilation of the ocean’s deepest water, *Paleoceanography*, 14, 571–588, 1999.
- 25 Toggweiler, J. R.: Origin of the 100,000-year time scale in Antarctic temperatures and atmospheric CO₂, *Paleoceanography*, 23, PA2211, doi:10.1029/2006PA001405, 2008.
- Weeding, B. and Trull, W.: Hourly oxygen and total gas tension measurements at the Southern Ocean time series site reveal winter ventilation and spring net community production, *Journal of Geophysical Research: Oceans*, 119, 348–358, 2004.
- Wolff, E., Barbante, C., Becagli, S., Bigler, M., Boutron, C., Castellano, E., de Angelis, M., Federer, U., Fischer, H., Fundel, F., Hansson, M., Hutterli, M., Jonsell, U., Karlin, T., Kaufmann, P., Lambert, F., Littot, G., Mulvaney, R., Roöthlisberger, R., Ruth, U., Severi, M., Siggaard-Andersen, M., Sime, L., Steffensen, J., Stocker, T., Traversi, R., Twarloh, B., Udisti, R., Wagenbach, D., and Wegner, A.: Changes in environment over the last 800,000 years from chemical analysis of the EPICA Dome C ice core, *Quaternary Science Reviews*, 29, 285–95, 2010.
- 30 Yu, J., Broecker, W., Elderfield, H., Jin, Z., McManus, J., and Zhang, F.: Loss of Carbon from the Deep Sea Since the Last Glacial Maximum, *Science*, 330, 1084–1087, 2010.
- 35 Yu, J., Anderson, R., Jin, Z., Rae, J., Opdyke, B., and Eggins, S.: Responses of the deep ocean carbonate system to carbon reorganization during the Last Glacial-interglacial cycle, *Quaternary Science Reviews*, 76, 39–52, 2013.



- Yu, J., Anderson, R., Z.Jin, Menviel, L., Zhang, F., Ryerson, F., and Rohling, E.: Deep South Atlantic carbonate chemistry and increased interocean deep water exchange during last deglaciation, *Quaternary Science Reviews*, 90, 80–89, 2014a.
- Yu, J., Anderson, R. F., and Rohling, E. J.: Deep ocean carbonate chemistry and glacial-interglacial atmospheric CO₂ changes, *Oceanography*, 27, 16–25, 2014b.
- 5 Yu, J., Menviel, L., Jin, Z. D., Thornalley, D., Barker, S., Marino, G., Rohling, E. J., Cai, Y., Zhang, F., Wang, X., Dai, Y., Chen, P., and Broecker, W. S.: Sequestration of carbon in the deep Atlantic during the last glaciation, *Nature Geoscience*, 9, 319–325, 2016.
- Yu, J., Menviel, L., Jin, Z., Thornalley, D., Foster, G., Rohling, E., McCave, I., McManus, J., Dai, Y., Ren, H., He, F., Zhang, F., Chen, P., and Roberts, A.: More efficient North Atlantic carbon pump during the Last Glacial Maximum, *Nature Communications*, 10, <https://doi.org/10.1038/s41467-019-10028-z>, 2019.
- 10 Zhao, N., Marchal, O., Keigwin, L., Amrhein, D., and Gebbie, G.: A Synthesis of Deglacial Deep-Sea Radiocarbon Records and Their (In)Consistency With Modern Ocean Ventilation, *Paleoceanography and Paleoclimatology*, 33, 128–151, 2017.